The paraventricular thalamus provides a polysynaptic brake on limbic CRF neurons to sex-dependently blunt binge alcohol drinking and avoidance behavior

Olivia B. Levine[1], Mary Jane Skelly[2], John D. Miller[2], Jeffrey F. DiBerto[3], Sydney A. Rowson[2], Jean K. Rivera-Irizarry[1], Thomas L. Kash[3], & Kristen E. Pleil[1,2,3,4,*]

[1]Graduate Program in Neuroscience, Weill Cornell Medicine, Cornell University
[2]Department of Pharmacology, Weill Cornell Medicine, Cornell University
[3]Department of Pharmacology and Bowles Center for Alcohol Studies, University of North Carolina-Chapel Hill School of Medicine
[4]Graduate Program in Pharmacology, Weill Cornell Medicine, Cornell University

*Corresponding author: krp2013@med.cornell.edu

Bed nucleus of the stria terminalis (BNST) neurons that synthesize and release the stress neuropeptide corticotropin-releasing factor (CRF) drive binge alcohol drinking and anxiety, behaviors that are primary risk factors for alcohol use disorder (AUD) and comorbid neuropsychiatric diseases more common in women than men. Here, we show that female C57BL/6J mice binge drink more than males and have greater basal $BNST^{CRF}$ neuron excitability and synaptic excitation. We identified a dense VGLUT2+ glutamatergic synaptic input from the paraventricular thalamus (PVT) that is anatomically similar in males and females. These PVT^{BNST} neurons release glutamate directly onto $BNST^{CRF}$ neurons but also engage a large BNST interneuron population to ultimately provide a net inhibition of $BNST^{CRF}$ neurons, and both components of this polysynaptic PVT^{VGLUT2}-$BNST^{CRF}$ circuit are more robust in females than males. While chemogenetic inhibition of the general PVT^{VGLUT2} neuron population suppressed binge alcohol drinking in both sexes, chemogenetic inhibition specifically of the PVT^{BNST} projection promoted this behavior in females without affecting males; chemogenetic activation of the pathway was sufficient to reduce avoidance behavior in both sexes in anxiogenic contexts. Lastly, we show that withdrawal from repeated binge drinking produces a female-like phenotype in the male PVT-$BNST^{CRF}$ excitatory synapse without altering the function of PVT^{BNST} neurons *per se*. Our data describe a complex and unique behavioral role of the feedforward inhibitory PVT^{VGLUT2}-$BNST^{CRF}$ glutamatergic circuit that is more robust in females and undergoes sex-dependent alcohol-induced plasticity.

Alcohol use disorder (AUD) is highly co-expressed with other neuropsychiatric diseases including anxiety disorders, with women having increased susceptibility to this comorbidity compared to men (61% vs 35%, respectively)[1]. Binge alcohol drinking is a primary risk factor for the development of these conditions, and females across mammalian species display greater binge drinking and transition from first alcohol use to disease states more quickly than males[2]. Females also exhibit exaggerated negative health consequences across peripheral and central tissues for every drink consumed[3]. These initial differences in alcohol sensitivity suggest that the mechanisms underlying early drinking contribute to disease susceptibility and are important targets for intervention[2]. The bed nucleus of the stria terminalis (BNST) is a hub in the brain circuits underlying anxiety and alcohol/substance use disorders in humans and is highly sexually dimorphic in mammals[4,5]. The BNST is enriched with neurons that synthesize and release corticotropin-releasing factor (CRF), a stress neuropeptide involved in the development and maintenance of anxiety and addictive disorders, and activation of $BNST^{CRF}$ neurons drives binge drinking behavior and produces anxiety[6,7]; however, the identity and organization of upstream excitatory circuits controlling $BNST^{CRF}$ neuron function and its role in alcohol drinking and anxiety are poorly understood. The BNST is anatomically connected to the paraventricular nucleus of the thalamus (PVT), a region likewise implicated in the etiology of alcohol and substance use disorders and associated behaviors including anxiety[8-11]. Human neuroimaging studies have demonstrated a functional connection between the thalamus and BNST that is denser in females than males[4,5] and decreased thalamic projection strength in young individuals with alcohol abuse[12]. These converging lines of evidence implicate a sex-dependent role for the PVT-BNST projection in behavior via modulation of $BNST^{CRF}$ neurons. Here, systematically examined in both sexes the anatomical and functional architecture of the PVT-$BNST^{CRF}$ circuit and its role in risky alcohol drinking and anxiety behaviors, as well as alcohol-induced plasticity.

First, we demonstrated that female C57BL/6J mice consistently consume more alcohol than males using the Drinking in the Dark (DID)[13,14] model of binge drinking (**Fig. 1a**). To determine whether this potentiated alcohol intake is related to increased excitability of $BNST^{CRF}$ neurons in females, we performed whole-cell patch-clamp slice electrophysiological recordings in CRF neurons in BNST slices from CRF-ires-Cre (CRF-Cre) x floxed Ai9 (CRF-Cre x Ai9) mice (**Fig. 1b**). We found that $BNST^{CRF}$ neurons were twice as likely to be firing in their basal state in females compared to males (40% in females vs. 17% in males; **Fig. 1c**). We also found that female

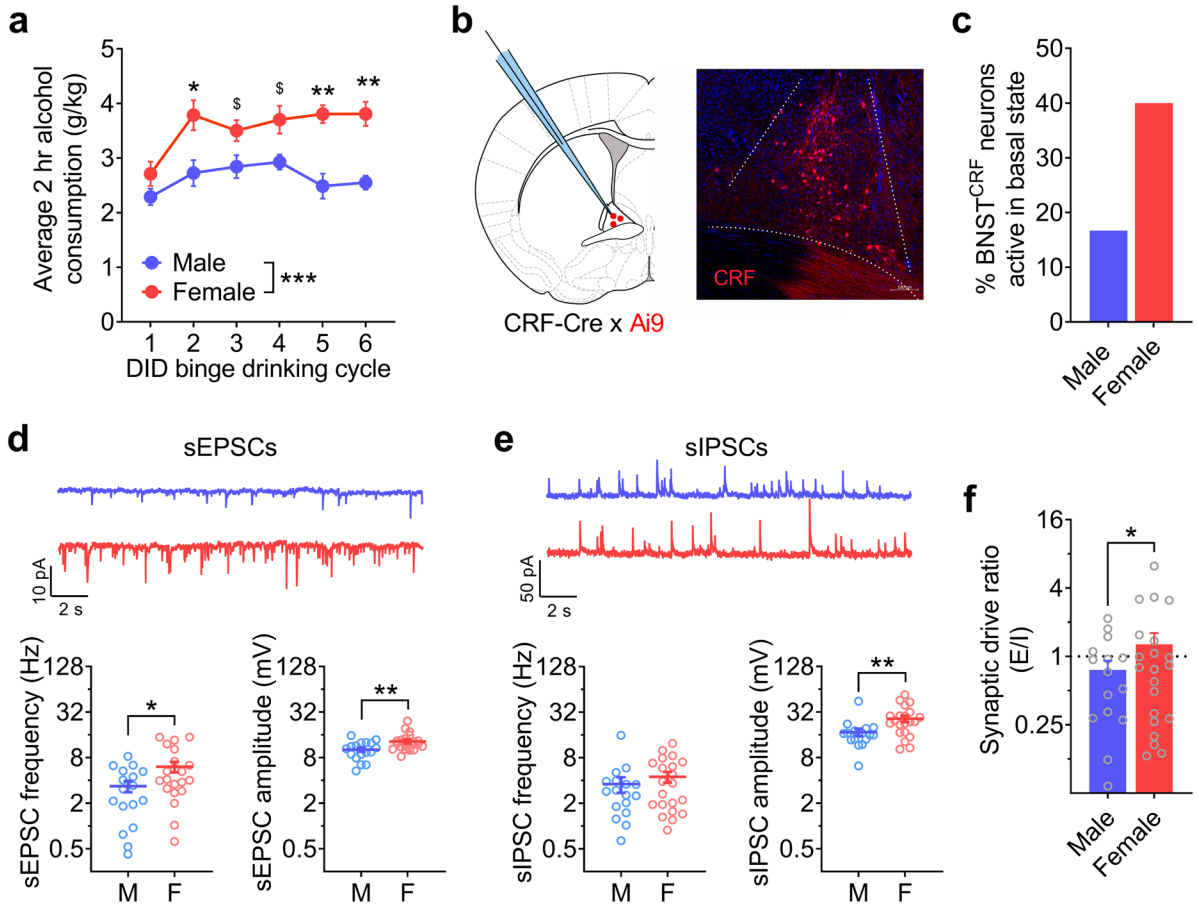

Fig. 1: Females display higher binge alcohol drinking and have greater BNST^{CRF} neuron excitation. a, Average 2-hr alcohol consumption across cycles of the Drinking in the dark (DID) binge drinking paradigm showing higher binge drinking in females than males (n = 10 male mice, 10 female mice). Two-way RM-ANOVA: main effect of sex ($F_{1,18}$ = 21.62, $^{***}P$ = 0.0002) and cycle ($F_{4,73}$ = 6.34, P = 0.0002, not indicated), but no interaction (P > 0.05); direct comparisons within-cycle show sex differences on cycle 2 ($t_{15.8}$ = 1.58, adjusted $^{*}P$ = 0.037), cycle 5 ($t_{16.3}$ = 4.71, adjusted $^{**}P$ = 0.001), and cycle 6 ($t_{14.5}$ = 4.96, adjusted $^{**}P$ = 0.001), with trends on cycle 3 ($t_{17.9}$ = 2.32, adjusted $^{\$}P$ = 0.063) and cycle 4 ($t_{13.9}$ = 2.67, adjusted $^{\$}P$ = 0.054). **b**, Schematic of whole-cell patch clamp recordings of CRF+ neurons in the BNST (BNST^{CRF} neurons, left) and representative 10x confocal image of a coronal BNST section from a CRF-Cre x Ai9 reporter (CRF-reporter) mouse. **c**, Proportion of BNST^{CRF} neurons sampled that fire in their basal state is greater in females than males (n = 10 male mice, 18 cells; 8 female mice, 19 cells). **d-f**, spontaneous excitatory and inhibitory synaptic transmission in male and female BNST^{CRF} neurons (males: n = 8 mice, 17 cells; females: n = 8 mice, 21 cells; unpaired t-tests). **d**, Top: representative traces of spontaneous excitatory postsynaptic currents (sEPSCs) in BNST^{CRF} neurons of males (blue, above) and females (red, below). Bottom: Quantification of sEPSC frequency (left, t_{36} = 2.20, $^{*}P$ = 0.034) and amplitude (right, t_{36} = 2.88, $^{**}P$ = 0.007). **e**, Top: Representative traces of spontaneous inhibitory postsynaptic currents (sIPSCs) in BNST^{CRF} neurons of males (blue, above) and females (red, below). Bottom: Quantification of sIPSC frequency (left, t_{36} = 0.89, P = 0.380) and amplitude (right, t_{36} = 3.66, $^{**}P$ = 0.007). **f**, Synaptic drive ratio, calculated as (sEPSC frequency x amplitude) / (sIPSC frequency x amplitude), in BNST^{CRF} neurons (t_{35} = 2.41, $^{*}P$ = 0.022).

BNST^{CRF} neurons display higher amplitude of spontaneous excitatory and inhibitory postsynaptic currents (sEPSCs and sIPSCs, respectively), suggesting increased postsynaptic responses to synaptic input, as well as higher sEPSC frequency but not sIPSC frequency, suggesting greater glutamate, but not GABA, release onto

female BNST^{CRF} neurons (**Fig. 1d,e**). These differences contributed to a higher synaptic drive ratio in BNST^{CRF} neurons of females than males (**Fig. 1f**), indicating greater synaptic excitation and excitability in this neuron population that may in turn promote increased binge alcohol drinking in females relative to males.

Next, to ascertain whether there are sex differences in the density of specific glutamatergic inputs that drive synaptic transmission onto BNST^{CRF} neurons, we injected a retrograde virus unilaterally into the BNST of VGLUT2-ires-Cre (VGLUT2-Cre) mice to label VGLUT2-positive and negative BNST-projecting neurons (**Fig. 2a**). We identified several known sources of excitatory input to the BNST, including a well-characterized input from the basolateral amygdala (BLA) shown to reduce avoidance behavior in males[15,16]. Unexpectedly, we found that the brain region with the densest projection to the BNST was the PVT, which was similarly robust in both sexes across the anterior-posterior extent of the PVT and enriched in the anterior-mid PVT (**Fig. 2b-d**, with all labeled projections, regardless of Cre expression, shown in green in **2b**, quantified in **2c** and **Extended Data Fig. 1a-d**, and presented in density heat maps in **Fig. 2d**). Nearly all labeled neurons in the PVT were VGLUT2+ (average in **Fig. 2e** and by Bregma coordinate in **Extended Data Fig. 1e**), indicating a nearly pure VGLUT2+ glutamatergic projection. To determine whether PVT^{VGLUT2} neurons play a role in binge drinking behavior, we injected a Cre-dependent virus expressing the kappa opioid receptor (KOR)-based Gi-coupled designer receptor exclusively activated by designer drug (DREADD; together termed Gi-KORD throughout)[17] or control (CON) virus into the PVT of VGLUT2-Cre mice (**Fig. 2f**). Following administration of the Gi-KORD specific ligand Salvinorin B (SalB; 17 mg/kg, s.c.), male and female mice expressing the Gi-KORD displayed blunted binge drinking behavior while those injected with the CON vector were unaffected (**Fig. 2g**). In contrast, SalB activation of the Gi-KORD did not alter sucrose drinking or avoidance behavior in the open field test (OF; **Extended Data Fig. 2**), suggesting that PVT^{VGLUT2} neurons drive alcohol binge drinking behavior specifically without altering reward seeking behavior or anxiety more generally. Whole-cell patch-clamp recordings of BNST-projecting PVT (PVT^{BNST}) neurons indicated no sex differences in the intrinsic or synaptic excitability of this neuron population apart from decreased sIPSC amplitude in females (**Extended Data Fig. 3**). Altogether, these data demonstrate that the role of the PVT in binge drinking behavior and anatomical and functional organization of the PVT^{VGLUT2}-BNST circuit are similar in males and females.

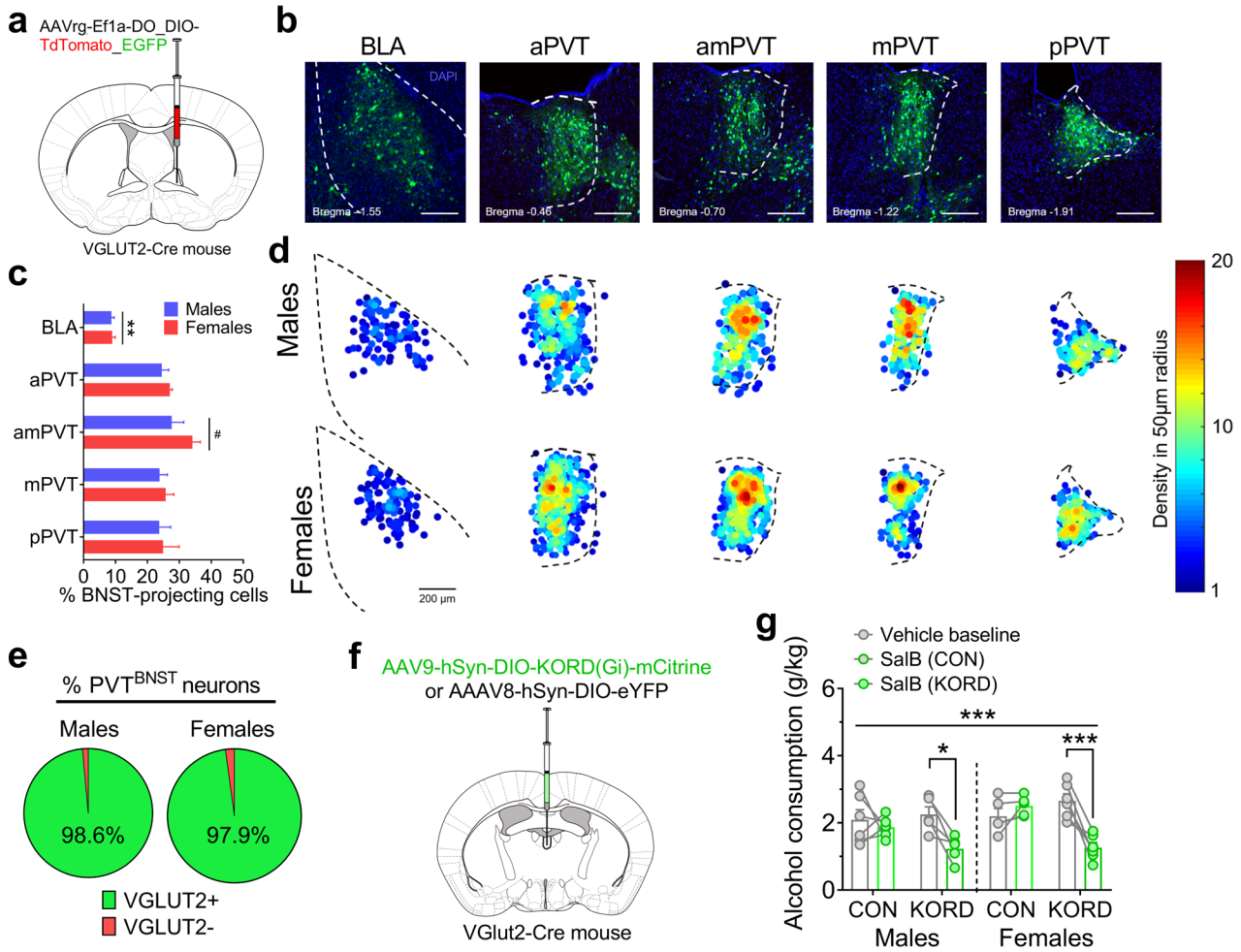

Fig. 2: The PVT provides a dense glutamatergic projection to the BNST and modulates binge drinking in both sexes. a-e, Illustration and quantification of BNST-projecting neurons in glutamatergic neuron regions. **a,** Schematic of intra-BNST delivery of a virus containing a retrogradely trafficked reporter vector (AAVrg-Ef1a-DO_DIO-TdTomato_EGFP-WPRE-pA) unilaterally into the BNST of VGLUT2-Cre mice to label distal neurons that project to the BNST (n = 4 male and 4 female mice). **b,** Representative images of coronal brain slices from a virus-injected mouse illustrating the expression of DAPI (blue) and all BNST-projecting cells (both VGlut2-Cre+ and – in green) in the basolateral amygdala (BLA) and across the A/P extent of the paraventricular nucleus of the thalamus (PVT), the densest sources of glutamatergic input identified. **c,** Quantification of % cells in BLA and PVT sections that project to the BNST, calculated as (total # of retrogradely-labeled cells / total DAPI count) x 100. Mixed-effects model: main effect of subregion ($F_{2.2,12.4}$= 32.01, $P < 0.0001$, not indicated) but no effect of sex or interaction (*P*s > 0.35); post hoc direct comparisons between subregions show that the BLA has fewer BNST-projecting neurons than the PVT across all A/P coordinates, with adjusted ***P*s < 0.01, and that the amPVT has more than the mPVT (t_7 = 3.82, adjusted $^{\#}P$ = 0.039). aPVT, anterior PVT; amPVT anterior-mid PVT; mPVT, mid PVT: pPVT, posterior PVT. **d,** Density heat maps illustrating the average number of BNST-projecting cell bodies within a 50 uM radius of each identified projection neuron for samples from each sex, matched and scaled similarly to representative images in **b,** illustrating the increased density of BNST-projecting across the PVT compared to the BLA that is similar between sexes (top: males, bottom: females). **e,** Proportion of VGLUT2-Cre+ (EGFP-labeled) and VGLUT2-Cre- (tdTomato-labeled) BNST-projecting PVT (PVT^{BNST}) neurons in males and females, showing that almost all PVT^{BNST} neurons are VGLUT2+ in both males and females. An unpaired t-test between males and females (t_6 = 1.24, P = 0.261) confirms there is no sex difference in the proportions. **f,** Schematic of viral strategy to express an inhibitory Gi-KOR DREADD (Gi-KORD) or control virus specifically in PVT^{VGLUT2} neurons. **g,** One-hr binge alcohol consumption during DID at within-cycle baseline including Day 2 vehicle injection (gray) and following Salvinorin B (SalB) injection (17 mg/kg, s.c., green) on Day 4 to activate the KORD (n = 5-6 mice/group). Three-way RM-ANOVA: main effects of the KORD ($F_{1,18}$ = 4.92, P = 0.037, not indicated) and SalB ($F_{1,18}$ =

16.17, $P = 0.0008$, not indicated), and a KORD x SalB interaction ($F_{1,18} = 18.51$, ***$P = 0.0004$); post hoc paired t-tests show that SalB administration blunts binge drinking in male and female mice with the KORD ($t_4 = 3.79$, adjusted *$P = 0.019$ and $t_5 = 5.29$, adjusted ***$P = 0.0003$, respectively) but not their control-virus counterparts (adjusted Ps > 0.15).

To establish whether there are sex differences in the function of the PVT-BNST (PVT^{BNST}) pathway and postsynaptic responses from $BNST^{CRF}$ neurons, we injected a CaMKIIα-driven channelrhodopsin (ChR2) virus into the PVT of CRF-Cre x Ai9 mice and recorded from $BNST^{CRF}$ neurons (**Fig. 3a,b**). We found that ChR2 activation of the PVT synaptic input (2 ms pulses, 490 nm LED) elicited an optically-evoked monosynaptic EPSC and polysynaptic IPSC (oEPSC and oIPSC, respectively) in $BNST^{CRF}$ neurons, as both currents could be abolished by bath application of the voltage-gated sodium channel blocker tetrodotoxin (TTX, 500 nM) but only the oEPSC was restored by addition of the voltage-gated potassium channel blocker 4-aminopyridine (4-AP, 100 μM; **Fig. 3c**). Quantification of oEPSC (**Fig. 3d**) and oIPSC (**Fig. 3e**) amplitudes across increasing LED power showed a more robust response in $BNST^{CRF}$ neurons from females compared to males; however, oIPSCs were larger than oEPSCs in most individual $BNST^{CRF}$ neurons in both sexes, suggesting that the net effect of PVT afferent activation is synaptic inhibition in both males and females (as evidenced by an excitatory/inhibitory (E/I) ratio below one, **Fig. 3f**). We next confirmed that activating PVT^{BNST} inputs results in a net inhibition of $BNST^{CRF}$ neurons using whole-cell current-clamp recordings, demonstrating that LED excitation of ChR2 from PVT terminals produced an optically-evoked postsynaptic potential (oPSP) that was on average hyperpolarizing (but variable across individual neurons; **Extended Data Fig. 4a,b**). This oPSP was depressed across increasing stimulation frequencies in males but not females (**Extended Data Fig 4c**).

Given the inhibitory effect of *ex vivo* PVT^{BNST} afferent activation on $BNST^{CRF}$ neuron excitability but our observation that *in vivo* activation of the PVT^{VGLUT2} population drives binge drinking comparably to activation of $BNST^{CRF}$ neurons[6,7], we next evaluated the specific role of the PVT^{BNST} circuit in binge drinking and anxiety-like behavior. We used a multiplexed chemogenetic strategy[17] to bidirectionally and independently manipulate the PVT^{BNST} circuit during behavior. We expressed either a cocktail of a Cre-dependent excitatory (hM3D) Gq-DREADD + Cre-dependent inhibitory Gi-KORD or a Cre-dependent CON vector in retrogradely Cre-labeled PVT^{BNST} neurons (**Fig. 3g,h; Extended Data Fig. 5a,b**). We found that CNO administration (5 mg/kg, i.p.) to activate the Gq-DREADD prior to alcohol access during Day 4 DID did not reliably alter binge consumption of

20% alcohol compared to vehicle baseline (**Fig. 3i);** however there was trend for a decrease in consumption in DREADD males, suggesting that activation of the PVT^{BNST} pathway is sufficient to blunt binge alcohol drinking in a subset of males (see **Extended Data Fig. 5c**). In contrast, Salvinorin B (SalB) administration (17 mg/kg, s.c.) to activate the Gi-KORD robustly increased binge alcohol drinking in DREADD females but had no effect in DREADD males or either CON group (**Fig. 3j, Extended Data Fig. 5d**), suggesting that tonic activity of the PVT^{BNST} circuit (**Extended Data Fig. 3c**) engaging interneurons is necessary for active suppression of alcohol drinking behavior in females. As $BNST^{CRF}$ neurons show larger postsynaptic responses to the PVT^{BNST} input in females (**Fig. 3d,e**), reducing the activity of the PVT^{BNST} input may result in a more robust polysynaptic disinhibition of $BNST^{CRF}$ neurons to further enhance binge drinking. Intriguingly, neither chemogenetic manipulation affected 1% sucrose consumption in a similar DID paradigm (**Extended Data Fig. 6a,b**). These results suggest that the PVT^{BNST} projection plays an opposing role in binge drinking behavior to the general PVT^{VGLUT2} glutamate neuron population (**Fig. 2g**) and one that is not dependent on modulation of the general rewarding or aversive aspects of drug intake and consummatory behavior previously shown to be mediated by other major limbic outputs of the PVT such as the nucleus accumbens[18-20].

We also probed whether the PVT^{BNST} circuit plays a role in anxiety-like behavior, given our previous work showing that activity of the $BNST^{CRF}$ neuron population is anxiogenic[21,22] and that the PVT regulates emotional behaviors[11,23]. CNO administration to activate the Gq-DREADD decreased avoidance of the open arms on the elevated plus maze (EPM) in DREADD mice compared to CON mice (**Fig. 3k, Extended Data Fig. 6c**), an anxiolytic effect of Gq-DREADD activation that we replicated in the open field test (OF; **Extended Data Fig. 6e,f**). In contrast, SalB administration to activate the Gi-KORD did not affect avoidance of the center of the open field (OF; **Fig. 3l, Extended Data Fig. 6d**). We confirmed that chemogenetic activation of the PVT^{BNST} circuit results in a net decrease in $BNST^{CRF}$ neuron activity using an *ex vivo* slice calcium imaging approach (**Extended Data Fig. 7**). Together, these results suggest that in an anxiogenic context when $BNST^{CRF}$ neuron activity is high[24,25], activation of the PVT^{BNST} synaptic brake is sufficient to decrease anxiety-like behavior.

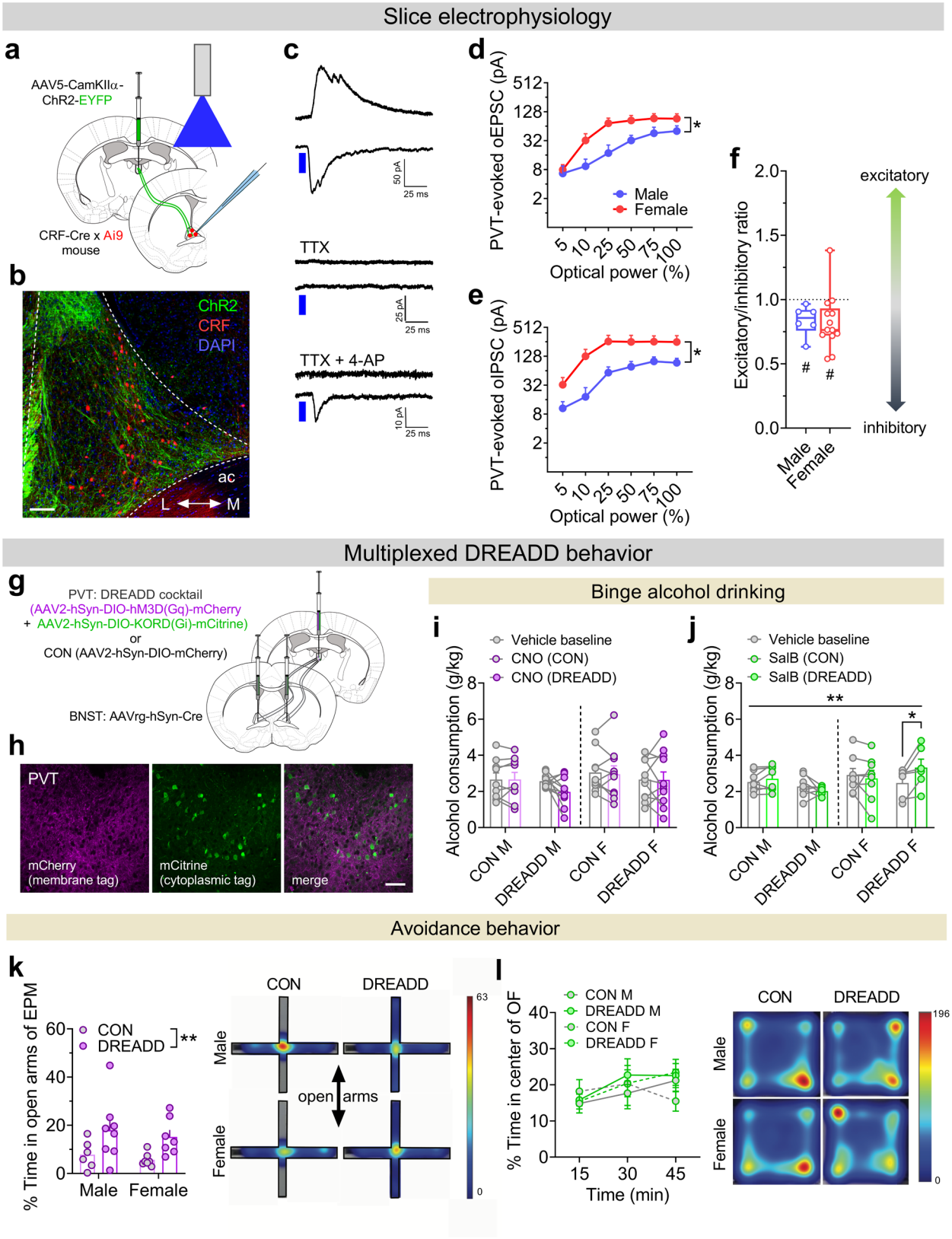

Fig. 3: The PVT-BNST projection provides polysynaptic inhibition onto BNST^{CRF} neurons and regulates binge alcohol drinking and avoidance behavior. a, Schematic illustrating the approach for whole-cell patch-clamp electrophysiology recordings in BNST^{CRF} neurons during optical excitation of ChR2 to elicit time-locked glutamate release from PVT axon terminals. **b**, Representative 20x image of the dorsal in a coronal slice using the viral strategy in **a** with DAPI counterstain; ac = anterior commissure, L = lateral, M = medial. Scale bar = 100 μM. **c**, Representative traces of a whole-cell recording from a BNST^{CRF} neuron demonstrating that a 2-ms

pulse of 490 nm light, indicated by blue line, elicits a time-locked optically-evoked EPSC and IPSC (oEPSC and oIPSC, respectively; top) from PVT terminals, which are abolished in the presence of tetrodotoxin (TTX, 1 μM; middle); a time-locked monosynaptic EPSC is restored with the addition of 4-aminopyridine (4-AP, 100 μM; bottom). **d-e,** LED power-response curves for oEPSCs (**d**) and oIPSCs (**e**) in the same $BNST^{CRF}$ neurons. Two-way RM-ANOVA for oEPSCs: main effect of power ($F_{2.9,48.8} = 48.7$, $P < 0.0001$) and a sex x power interaction ($F_{5,85} = 2.58$, $^*P = 0.032$), but no main effect of sex ($P > 0.10$); two-way RM-ANOVA for oIPSCs: main effect of power ($F_{2.5,43.1} = 54.1$, $P < 0.0001$) and a sex x power interaction ($F_{5,85} = 2.89$, $^*P = 0.019$), but no main effect of sex (P > 0.05). **f,** Ratio between the oEPSC and oIPSC elicited at 75-100% maximum LED power (E/I ratio) within individual $BNST^{CRF}$ neurons. One-sample t-tests show E/I ratios below the null hypothesis ratio of 1.0 in both males ($t_5 = 3.41$, $^*P = 0.019$) and females ($t_{12} = 2.90$, $^*P = 0.013$), demonstrating that the PVT-BNST input provides a net inhibition onto $BNST^{CRF}$ neurons. For **c-e**, n = 2 male mice, 6 cells; n = 6 female mice, 13 cells. **g,** Schematic illustrating the viral strategy for a multiplexed chemogenetic manipulation approach to bidirectionally manipulate the PVT-BNST (PVT^{BNST}) projection during behavior. **h,** Representative 40x image in the aPVT (midline, just ventral of the third ventricle) showing membrane labeling of the Gq-DREADD (mCherry fusion protein pseudo-colored in purple, left), cytoplasmic labeling of the Gi-KORD (separated cytoplasmic mCitrine tag in green, middle), and the merged image illustrating the coexpression of the two DREADD constructs in individual PVT^{BNST} neurons. Scale bar = 50 μM. **i-j,** Two-hr consumption of 20% alcohol in the DID paradigm during a within-cycle baseline (gray bars) and on Day 4 (colored bars) following vehicle or ligand administration 40 min prior to alcohol access in CON and DREADD cocktail-injected mice. **i**, CNO administration (5 mg/kg, i.p.) to activate the Gq-DREADD does not alter alcohol consumption, shown in a three-way RM-ANOVA: no effects of sex, DREADD, CNO, or any interactions between the variables (*P*s > 0.15, but see **Extended Data Fig. 5c**; N's = 9 CON M, 11 DREADD M, 10 CON F, 11 DREADD F). **j**, SalB administration (17 mg/kg, s.c.) to activate the KORD increases binge alcohol drinking in DREADD females but not males. Three-way RM-ANOVA shows a sex x DREADD x SalB interaction ($F_{1,26} = 8.76$, $^{**}P = 0.007$) but no main effects and no interactions between two variables (*P*s > 0.05); post hoc paired t-tests confirm that SalB increased alcohol consumption in DREADD females ($t_{26} = 3.08$, adjusted $^*P = 0.019$) but did not affect alcohol consumption in DREADD males or either control group (adjusted *P*s > 0.65). N's = 8 CON M, 8 DREADD M, 8 CON F, 6 DREADD F, with 0-3 mice excluded per group due to baseline drinking below criteria. **k**, CNO administration (5 mg/kg) decreases avoidance of the open arms on the elevated plus maze (EPM) in DREADD mice compared to CONs (quantified on left, with representative tracking heat maps on right). Two-way ANOVA on the percent time spent on the open arms shows a main effect of DREADD ($F_{1,24} = 9.30$, $^{**}P = 0.006$) but no effect of sex or a sex x DREADD interaction (*P*s > 0.45). Post hoc t-tests did not reveal significant differences between CON and DREADD groups specifically within each sex (adjusted *P*s > 0.05). N's = 6 CON M, 8 DREADD M, 7 CON F, 7 DREADD F. **l**, SalB administration (17 mg/kg) does not alter avoidance of the center of the open field (OF; quantified on left, with representative tracking heat maps on right). Three-way RM-ANOVA on the percent time spent in the center reveals a main effect of time ($F_{2,27.6} = 8.70$, $P = 0.003$, not indicated) but no other effects or interactions (*P*s > 0.10; N's = 4-5/group).

Finally, we examined the sex-dependent plasticity in this circuit following repeated binge alcohol drinking to understand whether there are changes in the PVT^{VGLUT2}-$BNST^{CRF}$ circuit during withdrawal that could contribute to increased disease vulnerability. Using the strategy described in **Fig. 3a**, we recorded from $BNST^{CRF}$ neurons one day after three cycles of EtOH DID (**Fig. 4a**). We found that the proportion of $BNST^{CRF}$ neurons in an active state was increased following EtOH exposure in both sexes, with EtOH males displaying a similar phenotype to CON females and EtOH females displaying an even greater proportion of active neurons (**Fig. 4b**). Notably, a range of neural activity patterns were observed in all groups, illustrating the heterogeneity of the $BNST^{CRF}$ population in both sexes as previously described in males[26,27]. Most other measures of intrinsic

excitability and current-injected firing were neither different between males and females nor altered following EtOH DID exposure when measured either at their resting membrane potential (RMP; **Extended Data Fig. 8**) or at a common hyperpolarized potential of -70 mV (**Extended Data Fig. 9**). Interestingly, this suggests that the primary effect of repeated alcohol exposure is on the population-level excitability of $BNST^{CRF}$ neurons, resulting in males displaying a female-like phenotype and females exhibiting a further potentiation of already elevated excitability levels. Examination of synaptic transmission showed that sEPSC frequency was increased in EtOH males to a level comparable to that observed in CON females, but this measure was unchanged by EtOH exposure in females (**Fig. 4c**), while sEPSC amplitude was unchanged in both sexes (**Fig. 4d**). Altogether, binge alcohol drinking increased excitatory synaptic drive onto $BNST^{CRF}$ neurons in males, thereby producing a female-like phenotype following EtOH exposure (**Fig. 4e**). In contrast, there were no changes in the frequency, amplitude, or synaptic drive of sIPSCs in either sex (**Fig 4f-h**). Examination of the kinetics of sPSCs revealed increased half-width and weighted tau of sEPSCs in EtOH males, consistent with an increase in glutamatergic transmission, as well as a sex difference in the rise time of sIPSCs, but no other effects (**Extended Data Fig. 10**).

We next examined plasticity in PVT-evoked postsynaptic responses from $BNST^{CRF}$ neurons and found that oEPSC amplitude was increased during withdrawal following repeated cycles of EtOH DID only in males (**Fig. 4i**). Specific analysis of the slope of the initial increase in oEPSC amplitude across increased LED power confirmed this EtOH-induced increase in the excitatory postsynaptic responses of $BNST^{CRF}$ neurons in males to female-like levels (**Fig. 4j**; **Extended Data Fig. 11a**), mirroring the EtOH effect on sEPSCs in males (**Fig. 4c-e**) and suggesting that PVT-$BNST^{CRF}$ synapses comprise a large contingent of the glutamate synapses vulnerable to EtOH-induced plasticity. However, this EtOH-induced potentiation of oEPSCs in males was met with an increase in polysynaptic oIPSCs (**Fig. 4k**), although the initial slope was similar across groups (**Fig. 4l**; **Extended Data Fig. 11b**). Intriguingly, following voluntary alcohol exposure, the E/I ratio of oPSCs remained significantly below one in males but not females (**Fig. 4m**), suggesting that while the overall E/I balance toward inhibition was maintained in males, the net inhibitory effect of PVT afferent activation at $BNST^{CRF}$ neurons was attenuated in females. Notably, we observed very few sex differences or alcohol-induced changes in the electrophysiological properties, excitability, and synaptic transmission of PVT^{BNST} neurons themselves

(**Extended Data Figs. 12 and 13**), suggesting that sex- and alcohol-dependent differences in the PVT-BNST^{CRF} synapse strength are not due to differences in PVT^{BNST} neuronal excitability *per se*. Together, our data suggest that the effects of sex and repeated binge alcohol drinking are on the tonic activity of the BNST^{CRF} neuron population, due to basal differences in and differential plasticity in PVT^{VGLUT2}-BNST^{CRF} synapses and BNST^{CRF} neuron responses to the largely tonically-active PVT^{BNST} afferents.

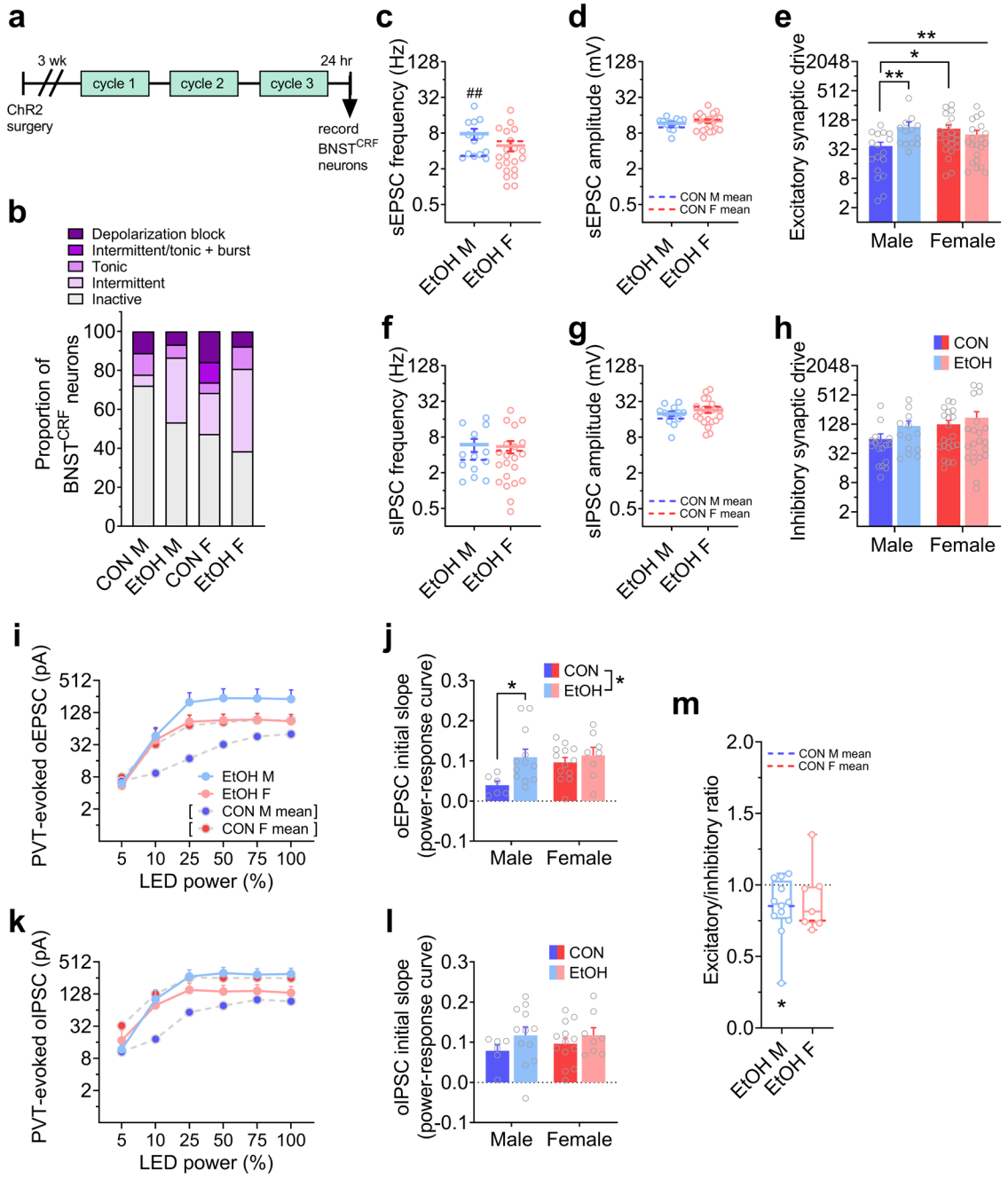

Fig. 4: A history of voluntary binge alcohol drinking induces a female-like phenotype in male BNST^{CRF} neurons and PVT-BNST^{CRF} synapses. a, Experimental timeline for recording from BNST^{CRF} neurons (as depicted in **Fig. 3a**) during withdrawal from three cycles of alcohol DID (EtOH) or a water DID control (CON) procedure (CONs are the same males and females presented in **Figs. 1 and 3**; means for CON cell data already shown are represented in this figure by dashed lines). **b**, Characterization of the types of neuronal

activity in BNST^{CRF} neurons, presented as % sampled population, showing that the basal excitability of the BNST^{CRF} neuron population is higher in both sexes following voluntary alcohol exposure, illustrated by larger subpopulations in states of firing in EtOH males and females compared to their water CONs. Ns = 6 EtOH M mice, 15 cells; 10 EtOH F mice, 26 cells. **c-d**, sEPSC frequency (**c**) and amplitude (**d**) in BNST^{CRF} neurons in EtOH M and EtOH F mice. Unpaired t-tests evaluating the effect of EtOH on sEPSC frequency show an effect of EtOH in males but not females: CON M vs. EtOH M (t_{28} = 3.08, $^{\#\#}P$ = 0.005), CON F vs. EtOH F (t_{40} = 1.02, P = 0.314); and sEPSC amplitude: CON M vs. EtOH M (t_{28} = 1.55, P = 0.132) and CON F vs. EtOH F (t_{40} = 0.520, P = 0.606). **e,** Excitatory synaptic drive, calculated as sEPSC frequency x sEPSC amplitude, within individual neurons. Two-way ANOVA: sex x EtOH interaction ($F_{1,68}$ = 10.55, $^{**}P$ = 0.002) but no main effects (Ps > 0.05); post hoc direct comparisons show a sex difference between CON M and F (t_{68} = 3.10, adjusted $^{*}P$ = 0.014) and effect of EtOH in males (t_{68} = 3.37, adjusted $^{**}P$ = 0.007) but not females (adjusted P > 0.50), demonstrating that EtOH increases spontaneous excitatory synaptic transmission in male BNST^{CRF} neurons to female levels. **f-g**, sIPSC frequency (**f**) and amplitude (**g**) in the same BNST^{CRF} neurons in **c** and **d**. Unpaired t-tests evaluating the effect of EtOH on sIPSC frequency show no effect of alcohol exposure: CON M vs. EtOH M (t_{28} = 1.63, P = 0.114), CON F vs. EtOH F (t_{40} = 0.025, P = 0.981); and sIPSC amplitude: CON M vs. EtOH M ($t_{17.2}$ = 1.49, P = 0.154) and CON F vs. EtOH F (t_{40} = 1.02, P = 0.314). **h**, Inhibitory synaptic drive, calculated as sIPSC frequency x sIPSC amplitude, within individual neurons. Two-way ANOVA: no effects or interactions (Ps > 0.30), confirming that neither sex nor alcohol exposure alter spontaneous inhibitory synaptic transmission in BNST^{CRF} neurons. For **c-h**, CON M and F cells are the same as those in **Fig. 1d-f**; 5 EtOH M mice, 13 cells; 8 EtOH F mice, 21 cells). **i,** Power-response curves for PVT-evoked oEPSCs. Three-way RM-ANOVA: main effect of power ($F_{2.5,87.8}$ = 86.4, P < 0.0001) and a trend for an EtOH x power interaction ($F_{5,175}$ = 2.25, P = 0.052), but no other effects or interactions (Ps > 0.15). **j**, Analysis of the initial slope of the power-oEPSC curve across increasing LED power (5-10-25%, where most change in evoked current occurred), calculated with linear regression. (Regressions for all individual neurons are shown in **Extended Data Fig. 11**.) Two-way ANOVA: main effect of EtOH ($F_{1,35}$ = 6.01, $^{*}P$ = 0.019) but no effect of sex or interaction (Ps > 0.05); post hoc t-tests show this effect of EtOH was driven by males (t_{35} = 2.64, adjusted $^{*}P$ = 0.025) but did not occur in females (P > 0.45). **k,** Power-response curve for oIPSCs. Three-way RM-ANOVA: main effect of power ($F_{2.4,85}$ = 103.4, P < 0.0001) and a sex x EtOH interaction ($F_{1,35}$ = 4.71, P = 0.037), but no other effects or interactions (Ps > 0.05), suggesting that EtOH differentially affected oIPSCs in males and females. **l,** Analysis of the initial slope of the LED power-oIPSC. Two-way ANOVA shows no effects (Ps > 0.10). **m,** E/I ratio within individual BNST^{CRF} neurons for EtOH M and EtOH F, with median values of CON groups from **Fig. 3f** represented with dashed lines for visual comparison. One-sample t-tests show that EtOH M have an E/I ratio below the null hypothesis ratio of 1.0 (t_{11} = 2.57, $^{*}P$ = 0.026) but EtOH F do not (t_{6} = 1.15, P = 0.30), suggesting that the ability of the PVT^{BNST} input to provide polysynaptic inhibition onto BNST^{CRF} neurons is attenuated in females following alcohol exposure. For **i-m**, CON M and F cells are the same as those in **Fig. 3d-f**; EtOH N's = 4 EtOH M mice, 12 cells and 3 EtOH F mice, 8 cells.

Altogether, we found that female mice display more robust binge drinking behavior than males and that BNST^{CRF} neurons are both more tonically active and receive increased excitatory synaptic input in females relative to males. We further demonstrated that the PVT provides a dense excitatory input to the BNST in both sexes that is more functionally robust in females than males, consistent with human neuroimaging studies[4,5]. We report that while PVT glutamate neurons directly synapse onto BNST^{CRF} neurons, they also provide robust feedforward inhibition of this population by recruiting interneurons, providing a synaptic "brake" on BNST^{CRF} neuron activity to actively suppress binge alcohol drinking, an important function in females. This PVT^{BNST} circuit plays a unique role in modulating drinking behavior that is directly opposed to the pro-drinking effect of general PVT glutamate neuron activation and is sex-dependent. In addition, activation of the PVT^{BNST} pathway

in aversive contexts, when BNST^{CRF} neuron activity is high[24,25], is sufficient to reduce avoidance behavior in both sexes. These results suggest a critical sex-dependent role of this thalamo-limbic circuit in the control of and relationship between risky alcohol drinking and anxiety states. Further, withdrawal from repeated binge drinking resulted in sex-dependent plasticity in the PVT^{VGLUT2}-BNST^{CRF} circuit, producing a female-like increased excitation in males and an attenuation of synaptic inhibition in females. Given the parallels with the human literature showing a reduction in thalamic projection density in those with a history of alcohol abuse, this circuit may be a target for intervention in individuals with risky binge drinking behaviors and resulting psychiatric diseases including AUD and anxiety disorders. Future studies will elucidate the molecular mechanisms by which these effects of sex and binge drinking contribute to the circuit mechanisms described here.

Methods

Subjects

All experimental mice were young (8-9 weeks of age at the onset of experiment) male and female adult mice on a C57BL/6J background strain. Wild-type C57BL/6J mice were purchased as adults from Jackson Laboratory, and all transgenic lines were bred in our animal facility. CRF-ires-Cre (CRF-Cre)[21,28] and VGLUT2-ires-Cre (VGLUT2-Cre)[29] mice were bred with WT C57BL/6J mice, and hemizygous CRF-Cre mice were bred with homozygous floxed Ai9-tdTomato mice (B6.Cg-*Gt(ROSA)26Sor*$^{tm9(CAG\text{-}tdTomato)Hze}$/J, stock #007909, Jackson Laboratory) to produce CRF-Cre$^{+/-}$ x Ai9$^{f/-}$ reporter mice. Mice were group housed with *ad libitum* access to food and water in colony room on a 12:12 hr reverse light cycle, with lights off at 7:30 a.m. Mice were singly housed for one week prior to the onset of behavioral experiments and remained singly housed thereafter. Experiments were performed approximately 3 hr into the dark phase of the light cycle. All experimental procedures were approved by the Institutional Animal Care and Use Committees at Weill Cornell Medicine and University of North Carolina-Chapel Hill.

Stereotaxic surgeries

For experiments requiring site-directed administration of viral vectors or retrobeads, mice were anesthetized with 2% isoflurane (VetEquip, Livermore, CA) in 0.8% oxygen in an induction chamber

(VetEquip, Livermore, CA) then placed in an Angle Two mouse stereotaxic frame (Leica Biosystems, Wetzlar, Germany) and secured with ear bars into a nose cone delivering isoflurane to maintain anesthesia. Mice were given a subcutaneous injection of meloxicam (2 mg/kg) for preemptive analgesia and 0.1 mL of 0.25% Marcaine around the incision site. A Neuros 7000 series 1 µL Hamilton syringe with 33-gauge needle (Reno, NV) connected to a remote automated microinfusion pump (KD Scientific, Holliston, MA) was used for construct delivery at a rate of 50-100 nL/min to the PVT (A/P: -0.82, M/L: 0.00, D/V: -3.25, 200 nL) or BNST (A/P: +0.3 mm, M/L: ±1.1 mm, D/V: −4.35 mm, 250 nL). Following infusion, the needle was left in place for 10 min and then slowly manually retracted to allow for diffusion and prevent backflow of virus. Mice were continuously monitored for at least 30 minutes post-surgery to ensure recovery of normal breathing pattern and sternal recumbency, and then checked daily.

Behavior assays

The standard Drinking in the Dark (DID) binge alcohol drinking paradigm was used in mice to model human binge consumption behavior[14]. For each cycle of EtOH DID, three hr into the dark cycle, the home cage water bottle was replaced with a bottle containing 20% (v/v) alcohol (EtOH) for two hr on Days 1-3 and four hr on Day 4, followed by three days of forced abstinence between consecutive cycles. A similar access schedule was used to evaluate binge sucrose consumption, except that home cage water bottles were replaced with 1% or 4% (w/v) sucrose. For all drinking experiments, empty “dummy” cages on the same rack as behavior mice received the same EtOH or sucrose bottle replacement, and consumption was adjusted for leak from dummy bottles and then normalized to bodyweight. The open field test (OF) was used to evaluate avoidance and locomotor behavior as previously described[21]. Mice were placed in the 50 x 50 cm arena for 60 min, and Ethovision video tracking (Noldus, Wageningen, Netherlands) was used to quantify raw locomotor and location data used to calculate measures including distance traveled and time spent in each compartment (center vs. periphery, total). The elevated plus maze (EPM) was also used to assess anxiety-like behaviors and was conducted in a plexiglass maze with two open and two closed arms (35 cm length x 5.5 cm width, with walls 15 cm tall over the closed arms). Mice were placed in the center of the EPM for five-minute trials and movement and time spent in each compartment was tracked using Ethovision. Total time and percent time spent in each arm were quantified.

in vivo chemogenetic manipulations

To examine the role of PVT^{VGLUT2} neurons in behavior, VGLUT2-Cre mice received a stereotaxic injection into the PVT (A/P: -0.82, M/L: 0.00, D/V: -3.25, 200 nL) of the kappa opioid receptor G_i-coupled Designer Receptor Exclusively Activated by Designer Drugs (Gi-KOR DREADD, or Gi-KORD) AAV9-hSyn-DIO-HA-KORD-IRES-mCitrine (gift from Bryan Roth) or control vector AAV8-hSyn-DIO-EYFP into the PVT (200 nL; **Fig. 2f**). To examine the specific role of the PVT^{BNST} projection in binge drinking and avoidance behavior, C57BL/6J mice received injections of a retrograde Cre virus (AAVrg-hSyn-HI.EGFP-Cre.WPRE.SV40 or AAVrg pmSyn1-EBFP-Cre) bilaterally in the BNST (A/P: +0.3 mm, M/L: ±1.1 mm, D/V: −4.35 mm, 250 nL), followed by a single midline PVT injection of either: a) a 1:1 cocktail of the excitatory Gq-DREADD AAV2-hSyn-DIO-hM3D(Gq)-mCherry (125 nL) plus inhibitory Gi-KORD AAV2-hSyn-DIO-KORD(Gi)-mCitrine (125 nL) or b) control virus AAV2-hSyn-DIO-mCherry (250 nL, **Fig. 3g,h**). Approximately one week following surgery, mice started the DID procedure with a baseline cycle followed by a cycle in which they received 0.9% sterile saline vehicle (10 ml/kg, i.p.) injections on Days 2 and 4 forty min prior to alcohol access to habituate to the injection procedure. Chemogenetic manipulations began the next cycle with saline on Day 2 and clozapine-n-oxide (CNO, 5 mg/kg in 0.9% saline) on Day 4. The KORD was subsequently evaluated similarly with a DMSO vehicle (1 ml/kg, s.c.) injection cycle and manipulation cycle with Salvinorin B (SalB, 17 mg/kg in DMSO). Mice displaying injection stress defined by > 1g/kg reduction in and < 1g/kg vehicle baseline drinking were excluded from analysis. For the OF and EPM, half of the animals of each sex received vehicle and half received the DREADD activator (CNO or SalB) 40 min prior to the assay. For sucrose DID, the same SalB or CNO drug administration procedure was used as that for EtOH DID.

Brain extraction and fluorescence immunohistochemistry

Following behavior procedures, mice were deeply anesthetized with pentobarbital (100 mg/kg, i.p.) and transcardially perfused with sterile phosphate-buffered saline (PBS) followed by 4% paraformaldehyde (PFA). Brains were extracted, post-fixed overnight in 4% PFA, and then placed in PBS until they were sliced on the coronal plane in 45 µm sections on a VT1000S vibratome (Leica Biosystems) to check injection placements and viral expression (hit maps of these expression data are presented in **Extended Data Fig. 5a,b**). To amplify the expression of fluorophore tags, coronal slices containing the PVT and BNST

from DREADD and CON mouse brains underwent immunofluorescence staining. Slices were washed twice in PBS followed by 0.2% triton (Fisher Bioreagents, Hampton, NH) for 10 minutes each and then blocked in 5% normal donkey serum (NDS) for 30 minutes. Tissue was incubated in primary antibody (DsRed rabbit polyclonal 1:400, Takara, Kusatsu, Japan) overnight at room temperature. The next day, slices were washed 3 times in 0.2% triton for 10 minutes each and then blocked in 5% NDS for 30 minutes. Tissue was then incubated in secondary antibody (Alexafluor-568 donkey anti-rabbit, 1:250, Invitrogen, Carlsbad, CA) for 2 hours and subsequently washed twice in 0.2% Triton and then in PBS for 10 minutes each. Slices were counterstained with DAPI, and mounted on slices and coverslipped with Vectashield hardmount antifade mounting medium (Vector Labs, Burlingame, CA) and stored in the dark at 4°C until imaged (as described below) to verify surgical placements and viral expression.

Retrograde neuronal tracing

For anatomical circuit tracing of excitatory inputs to the BNST, VGLUT2-Cre mice received stereotaxic injections of a retrograde virus (AAVrg-Ef1a-DO-DIO-TdTomato_EGFP-WPRE-pA) unilaterally into the BNST, which was is retrogradely trafficked to ultimately express GFP in Cre+ cells and tdTomato in Cre- cells that project to the BNST. Following three weeks to allow for optimal viral expression, mice were sacrificed and their brains harvested for quantification as described below.

Image acquisition and analysis

Coronal brain slices were collected and imaged for all experiments to confirm and quantify viral expression and immunolabeling. Images were acquired on a Zeiss LSM 880 Laser Scanning Confocal microscope (Carl Zeiss, Oberkochen, Germany). For the retrograde tracing experiment, images of the PVT and BLA were quantified using ImageJ (US National Institute of Health) to count the total number of DAPI-stained nuclei, GFP+ and tdTomato+ cells. The coordinates of each cell were analyzed using custom a MATLAB (MathWorks, Natick, MA) program and normalized to the most dorsomedial point of the PVT. Heatmaps of the density of BNST-projecting neurons were generated as described elsewhere[30], overlaying data from four mice per sex. The proportion of PVT projectors that are VGLUT2+ was calculated as GFP+ / (GFP+ plus tdTomato+).

Coordinates analyzed (mm from Bregma): BLA (-1.55), anterior (aPVT, -0.46mm), anterior-mid (am-PVT, -0.70), mid (mPVT, -1.22), and posterior (pPVT, -1.91).

ex vivo electrophysiological recordings

Slice electrophysiology experiments were performed as previously described[6,21]. Mice were decapitated under isoflurane anesthesia and their brains rapidly extracted. Coronal BNST slices (300 µm) were prepared on a VT1200 vibratome (Leica Biosystems) in ice-cold, oxygenated (95% O_2/5% CO_2) sucrose artificial cerebrospinal fluid (aCSF) containing (in mM): 194 sucrose, 20 NaCl, 4.4 KCl, 2 CaCl2, 1 Mg Cl2, 1.2 NaH2PO4, 10 glucose, and 26 NaHCO3 (pH 7.3 and 30 mOsm). Slices were transferred to a holding chamber with 30 °C oxygenated normal aCSF (in mM):124 NaCl, 4.4 KCl, 2 CaCl2, 1.2 MgSO4, 1 NaH2PO4, 10 glucose, and 26 NaHCO3 (pH 7.3 and 30 mOsm) and allowed to equilibrate for at least one hour. For electrophysiological recordings, slices were transferred to a submerged recording chamber (Warner Instruments, Hamden, CT) and perfused at a rate of 2 mL/min with 30°C oxygenated normal aCSF.

$BNST^{CRF}$ neurons were identified for recording with their tdTomato (Ai9) tag using a 580 nm LED under 40x objective (Olympus, Tokyo, Japan). Signals were acquired using a Multiclamp 700B amplifier (Molecular Devices), digitized, and analyzed via pClamp 10.4 software (Molecular Devices). Input resistance and access resistance were continuously monitored throughout experiments, and cells in which access resistance changed by more than 20% were not included in data analysis. Data were analyzed in Clampfit 10.7. Excitability experiments were performed in current-clamp configuration using a potassium gluconate-based intracellular recording solution containing (in mM): 135 KGluc, 5 NaCl, 2 $MgCl_2$, 10 HEPES, 0.6 EGTA, 4 Na-ATP and 0.4 Na-GTP (pH 7.3 and 280 mOsm). Synaptic transmission was measured in voltage-clamp configuration using a cesium-methanesulfonate-based intracellular recording solution containing (in mM): 135 CsMeth, 10 KCl, 10 HEPES, 1 $MgCl_2 \cdot 6H2O$, 0.2 EGTA, 4 Mg-ATP, 0.3 Na_2GTP, 20 phosphocreatine (pH 7.3, 280 mOsm).

Individual neurons were voltage clamped at -55 mV and then at +10 mV to isolate spontaneous EPSCs and IPSCs, respectively. Prior to slice electrophysiology experiments, mice underwent three cycles of EtOH DID

(EtOH group) or a water control DID procedure in which the replacement bottle contained water instead of EtOH (CON group) to allow for investigation of basic sex differences in function as well as for direct comparison to EtOH mice. Twenty-four hr following the onset of the last EtOH or water bottle access, mice were sacrificed for slice electrophysiology experiments as described above. For experiments investigating PVT^{BNST} neurons, mice received bilateral intra-BNST injections of green or red retrobeads (250 nL, Lumafluor) prior to DID to label this population for identification during recordings. For experiments characterizing postsynaptic responses in $BNST^{CRF}$ neurons to PVT glutamate inputs, mice received an intra-PVT stereotaxic injection of AAV5-CamKIIα-hChR2(H134R)-eYFP.WPRE.hGH (200 nL, Penn Vector Core and Addgene) three weeks prior to DID procedures. During recordings, 1 ms 490 nm LED stimulation was used to optically stimulate ChR2+ PVT cell bodies to elicit action potentials to confirm sufficient PVT expression and ChR2 fidelity at 1, 2, 5, 10, 20, and 50 Hz. One 2 ms stimulation every 10 s was used in the BNST to optically-evoke glutamate release from PVT terminals while recording postsynaptic responses from $BNST^{CRF}$ neurons in voltage-clamp, and 2 ms stimulation at 1, 2, 5, 10, and 20 Hz was used while measuring postsynaptic potentials in $BNST^{CRF}$ neurons in current-clamp.

ex vivo chemogenetics and calcium sensor imaging

CRF-Cre mice received bilateral intra-BNST injections of the calcium sensor GCaMP6s (AAV4-Syn-FLEX-GCaMP6s; UPenn Vector Core; 500 nL) and an intra-PVT injection of the excitatory hM3D DREADD virus (AAV8-CaMKIIα-hM3D(Gq)-mCherry, 200 nL) or control virus (AAV8-CaMKIIα-mCherry; **Extended Data Fig. 7c**). Four weeks later, fresh brain slices were acutely prepared as described for slice electrophysiology recordings above. GCaMP6s was excited with 35% 470 nm LED (CoolLED) at a frequency of 1 Hz for 10 s every min to minimize photobleaching, and videos were acquired at a frame rate of 10 Hz with an optiMOS monochrome camera (QImaging, Surrey, British Columbia, Canada), across the entire experiment including a five min baseline, 10 min bath application of CNO (10 μM), and 10 min washout period. The experimenter maintained objective focus on the BNST z-plane of interest containing several $CRF^{GCaMP6s}$ neurons throughout the experiment. Custom MATLAB code was used to analyze changes in fluorescence intensity in individual CRF^{GCaMP6} neurons (ΔF) compared to background fluorescence within the frame (intensity of entire field of view, F) throughout the video. $CRF^{GCaMP6s}$ cells from CON virus mice were used to quantify

the inherent linear decay in fluorescence of GCaMP6s, and fluorescence in hM3D CRF^{GCaMP6s} cell fluorescence was normalized to this decay for statistical analysis.

Statistical analyses

Statistical analyses were performed in GraphPad Prism 8, R, and MATLAB. Data for all dependent measures were examined for their distributions in normal and log space, outliers, and equality of variance across groups using Q-Q plots. Electrophysiological properties and synaptic transmission data were lognormally distributed, analyzed using log-transformed values, and presented as raw values on a log2 scale in figures; all other data were normally distributed, analyzed in raw space, and presented on a linear scale in figures. Outliers according to Q-Q plots were excluded (however this was rare and reported). Data are presented as mean ± SEM, with the exception of E/I ratios that are presented as median ± max/min value; raw data points are included in all figures except those with more than two repeated measures (because there are too many raw data points to be clearly represented).

Two-way analysis of variance (ANOVA) and unpaired t-tests were used to evaluate the effects of sex and alcohol on synaptic transmission and excitability data. Repeated measures ANOVAs (RM-ANOVAs) were used to examine the effects of treatment, cycles of binge drinking, different anatomical subregions, etc., within individual animals across experimental groups; mixed effects models were used when one or more matched data point was unavailable for an individual animal. To prevent false positive results and overinterpretation of data for RM-ANOVAs with three or more repeated measures within animal, sphericity was not assumed and the Geisser and Greenhouse correction of degrees of freedom was employed for the repeated measure. For all ANOVAs, significant effects were further probed with appropriate post hoc paired or unpaired t-tests with Holm-Sidak (H-S) correction for multiple comparisons, and multiplicity-adjusted p values are reported as indicated. Statistical comparisons were always performed with an alpha level of 0.05 and using two-tailed analyses.

Acknowledgements

We thank Bryan Roth for contributing DREADD viruses and Bradford Lowell for sharing VGLUT2-ires-Cre and CRF-ires-Cre mouse lines bred in our facilities for these studies. We also thank Alexis Kendra, Nakul Yadav,

and Avanti Shirke for their technical assistance. This research was supported by: NIH grants K99/R00 AA023559 and R01 AA027645, a NARSAD Young Investigator Award, a Stephen and Anna Maria Kellen Foundation Junior Faculty Award (KEP); NIH grants P60 AA011605, R01 AA019454, and U01 AA020911 (TLK); NIH grant T32 DA039080 (OBL); and NIH grant F32 AA025530 (MJS).

Author Contributions

KEP and TLK designed and oversaw all experiments. OBL, MJS, and KEP collected and analyzed slice electrophysiology data. OBL, JDM, JFD, SAR, JKRI, and KEP performed and analyzed behavior data. JDM collected and analyzed anatomical tracing data. JFD and JDM bred mice for all studies. KEP and OBL wrote the manuscript. All authors edited and approved the final version of the manuscript.

References

1 Kessler, R. C. *et al.* Lifetime co-occurrence of DSM-III-R alcohol abuse and dependence with other psychiatric disorders in the National Comorbidity Survey. *Archives of general psychiatry* **54**, 313-321 (1997).

2 McHugh, R. K., Votaw, V. R., Sugarman, D. E. & Greenfield, S. F. Sex and gender differences in substance use disorders. *Clinical psychology review* **66**, 12-23, doi:10.1016/j.cpr.2017.10.012 (2018).

3 White, A. M., Castle, I. P., Hingson, R. W. & Powell, P. A. Using Death Certificates to Explore Changes in Alcohol-Related Mortality in the United States, 1999 to 2017. *Alcohol Clin Exp Res* **44**, 178-187, doi:10.1111/acer.14239 (2020).

4 Avery, S. N., Clauss, J. A. & Blackford, J. U. The Human BNST: Functional Role in Anxiety and Addiction. *Neuropsychopharmacology : official publication of the American College of Neuropsychopharmacology* **41**, 126-141, doi:10.1038/npp.2015.185 (2016).

5 Avery, S. N. *et al.* BNST neurocircuitry in humans. *NeuroImage* **91**, 311-323, doi:10.1016/j.neuroimage.2014.01.017 (2014).

6 Pleil, K. E. *et al.* Effects of chronic ethanol exposure on neuronal function in the prefrontal cortex and extended amygdala. *Neuropharmacology* **99**, 735-749, doi:10.1016/j.neuropharm.2015.06.017 (2015).

7 Rinker, J. A. *et al.* Extended Amygdala to Ventral Tegmental Area Corticotropin-Releasing Factor Circuit Controls Binge Ethanol Intake. *Biol Psychiatry*, doi:10.1016/j.biopsych.2016.02.029 (2016).

8 Millan, E. Z., Ong, Z. & McNally, G. P. Paraventricular thalamus: Gateway to feeding, appetitive motivation, and drug addiction. *Progress in brain research* **235**, 113-137, doi:10.1016/bs.pbr.2017.07.006 (2017).

9 Hua, R. *et al.* Calretinin Neurons in the Midline Thalamus Modulate Starvation-Induced Arousal. *Curr Biol* **28**, 3948-3959.e3944, doi:10.1016/j.cub.2018.11.020 (2018).

10 Huang, A. S., Mitchell, J. A., Haber, S. N., Alia-Klein, N. & Goldstein, R. Z. The thalamus in drug addiction: from rodents to humans. *Philosophical transactions of the Royal Society of London. Series B, Biological sciences* **373**, doi:10.1098/rstb.2017.0028 (2018).

11 Kirouac, G. J. Placing the paraventricular nucleus of the thalamus within the brain circuits that control behavior. *Neurosci Biobehav Rev* **56**, 315-329, doi:10.1016/j.neubiorev.2015.08.005 (2015).

12 Bava, S., Jacobus, J., Thayer, R. E. & Tapert, S. F. Longitudinal changes in white matter integrity among adolescent substance users. *Alcoholism, clinical and experimental research* **37 Suppl 1**, E181-189, doi:10.1111/j.1530-0277.2012.01920.x (2013).

13 Rhodes, J. S., Best, K., Belknap, J. K., Finn, D. A. & Crabbe, J. C. Evaluation of a simple model of ethanol drinking to intoxication in C57BL/6J mice. *Physiology & behavior* **84**, 53-63, doi:10.1016/j.physbeh.2004.10.007 (2005).

14 Thiele, T. E., Crabbe, J. C. & Boehm, S. L., 2nd. "Drinking in the Dark" (DID): a simple mouse model of binge-like alcohol intake. *Current protocols in neuroscience* **68**, 9.49.41-12, doi:10.1002/0471142301.ns0949s68 (2014).

15 Kim, S. Y. *et al.* Diverging neural pathways assemble a behavioural state from separable features in anxiety. *Nature* **496**, 219-223, doi:10.1038/nature12018 (2013).

16 Crowley, N. A. *et al.* Dynorphin Controls the Gain of an Amygdalar Anxiety Circuit. *Cell reports* **14**, 2774-2783, doi:10.1016/j.celrep.2016.02.069 (2016).

17 Vardy, E. *et al.* A New DREADD Facilitates the Multiplexed Chemogenetic Interrogation of Behavior. *Neuron* **86**, 936-946, doi:10.1016/j.neuron.2015.03.065 (2015).

18 Reed, S. J. *et al.* Coordinated Reductions in Excitatory Input to the Nucleus Accumbens Underlie Food Consumption. *Neuron* **99**, 1260-1273.e1264, doi:10.1016/j.neuron.2018.07.051 (2018).

19 Neumann, P. A. *et al.* Cocaine-Induced Synaptic Alterations in Thalamus to Nucleus Accumbens Projection. *Neuropsychopharmacology* **41**, 2399-2410, doi:10.1038/npp.2016.52 (2016).

20 Zhu, Y., Wienecke, C. F., Nachtrab, G. & Chen, X. A thalamic input to the nucleus accumbens mediates opiate dependence. *Nature* **530**, 219-222, doi:10.1038/nature16954 (2016).

21 Pleil, K. E. *et al.* NPY signaling inhibits extended amygdala CRF neurons to suppress binge alcohol drinking. *Nat Neurosci* **18**, 545-552, doi:10.1038/nn.3972 (2015).

22 Marcinkiewcz, C. A. *et al.* Serotonin engages an anxiety and fear-promoting circuit in the extended amygdala. *Nature* **537**, 97-101, doi:10.1038/nature19318 (2016).

23 Penzo, M. A. *et al.* The paraventricular thalamus controls a central amygdala fear circuit. *Nature* **519**, 455-459, doi:10.1038/nature13978 (2015).
24 Salimando, G. J., Hyun, M., Boyt, K. M. & Winder, D. G. BNST GluN2D-containing NMDA receptors influence anxiety- & depressive-like behaviors and modulate cell-specific excitatory/inhibitory synaptic balance. *J Neurosci*, doi:10.1523/jneurosci.0270-20.2020 (2020).
25 Silberman, Y. & Winder, D. G. Emerging role for corticotropin releasing factor signaling in the bed nucleus of the stria terminalis at the intersection of stress and reward. *Front Psychiatry* **4**, 42, doi:10.3389/fpsyt.2013.00042 (2013).
26 Silberman, Y., Matthews, R. T. & Winder, D. G. A corticotropin releasing factor pathway for ethanol regulation of the ventral tegmental area in the bed nucleus of the stria terminalis. *The Journal of neuroscience : the official journal of the Society for Neuroscience* **33**, 950-960, doi:10.1523/jneurosci.2949-12.2013 (2013).
27 Vranjkovic, O., Pina, M., Kash, T. L. & Winder, D. G. The bed nucleus of the stria terminalis in drug-associated behavior and affect: A circuit-based perspective. *Neuropharmacology* **122**, 100-106, doi:10.1016/j.neuropharm.2017.03.028 (2017).
28 Krashes, M. J. *et al.* An excitatory paraventricular nucleus to AgRP neuron circuit that drives hunger. *Nature* **507**, 238-242, doi:10.1038/nature12956 (2014).
29 Vong, L. *et al.* Leptin action on GABAergic neurons prevents obesity and reduces inhibitory tone to POMC neurons. *Neuron* **71**, 142-154, doi:10.1016/j.neuron.2011.05.028 (2011).
30 Beyeler, A. *et al.* Organization of Valence-Encoding and Projection-Defined Neurons in the Basolateral Amygdala. *Cell reports* **22**, 905-918, doi:10.1016/j.celrep.2017.12.097 (2018).

Extended Data Figures

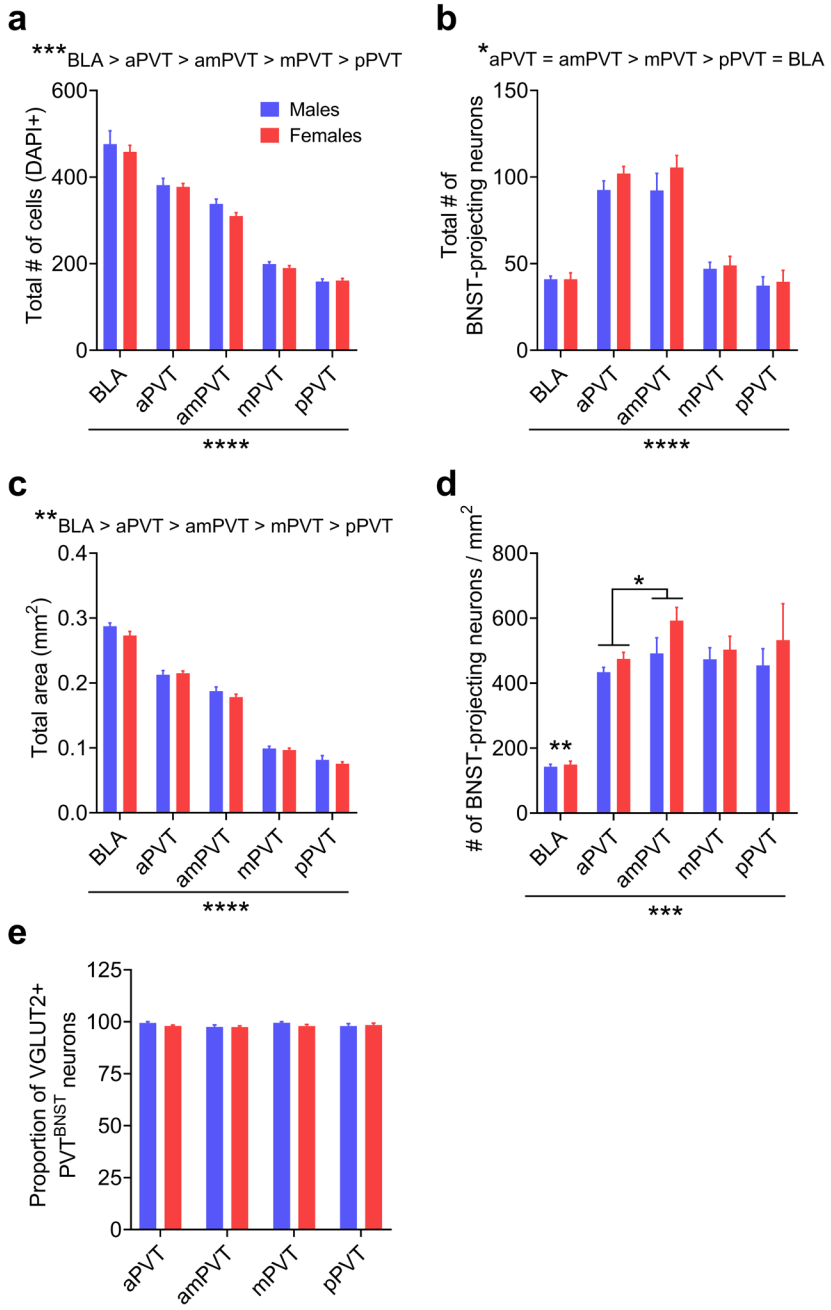

Extended Data Fig. 1: Detailed quantification of glutamatergic inputs to the BNST (related to Fig. 2a-e). **a,** Total number of cells per region/subregion in both sexes, indicated by a DAPI counterstain of nuclei. Mixed-effects model: main effect of subregion ($F_{1.4,8.2}$ = 324.0, ****P < 0.0001) but no effect of sex or interaction (Ps > 0.25), with BLA > aPVT > amPVT > mPVT > pPVT according to post hoc t-tests (adjusted ***Ps < 0.001 for all direct subregion comparisons). **b,** Total raw number of BNST-projecting neurons across subregions. Mixed-effects model: main effect of subregion ($F_{2.2,12.6}$ = 111.1, ****P < 0.0001) but no effect of sex or interaction (Ps > 0.30), with aPVT = amPVT > mPVT > pPVT = BLA according to post hoc t-tests (adjusted Ps < 0.05 for all significantly different subregion comparisons). **c,** Total area of each subregion. Mixed-effects model: main effect of subregion ($F_{2.6,19.6}$ = 559.9, ****P < 0.0001) but no effect of sex or interaction (Ps > 0.05), with BLA > aPVT > amPVT > mPVT > pPVT according to post hoc t-tests (adjusted **Ps < 0.01 for all direct subregion comparisons). **d,** Number of BNST-projecting neurons normalized to subregion area. Mixed-effects model: main effect of subregion ($F_{1.5,8.6}$ = 28.83, ***P = 0.0003) but no effect of sex or interaction (Ps > 0.20), with BLA < all PVT subregions (adjusted **Ps < 0.01) and aPVT < amPVT (adjusted *P = 0.040). **e,** Proportion of PVT^{BNST} neurons that are VGLUT2+ (**Fig. 2e** broken down by A/P subregion, with all sex x subregion proportions > 97.4%. Two-way RM-ANOVA shows no effects or interaction (Ps > 0.25).

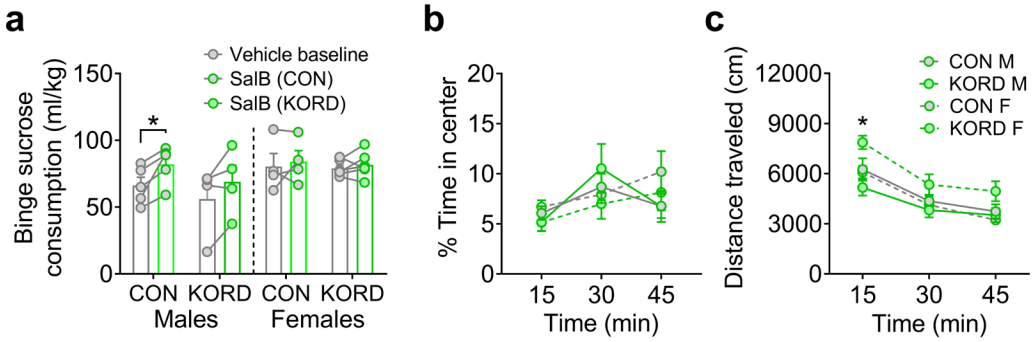

Extended Data Fig. 2: Lack of effects of chemogenetic activation of PVT^{VGlut2} neurons on binge sucrose consumption, anxiety, and locomotion (related to Fig. 2). a, One-hr sucrose consumption during a matched 4% sucrose DID procedure to **Fig. 2g** in KORD and control vector-expressing mice (n = 4-6 mice/group, with 0-1 excluded mouse/group with no baseline sucrose consumption). Three-way RM-ANOVA: main effect of SalB ($F_{1,15}$ = 11.88, P = 0.004) and a SalB x sex interaction ($F_{1,15}$ = 4.79, P = 0.045) but no effect of the KORD or sex or other interactions between the three variables (Ps > 0.05); paired t-tests show that the effect of SalB was driven by CON males (t_4 = 3.54, adjusted *P = 0.024; all others P > 0.10). **b-c**, Effects of SalB activation of the Gi-KORD in PVT^{VGLUT2} neurons on behavior in the OF. **b,** Percent time in center of the OF 40 min following SalB administration in KORD and control vector-expressing mice. Three-way RM-ANOVA: main effect of time ($F_{1.9,32.4}$ = 6.05, P = 0.007) and a sex x time interaction ($F_{2,34}$ = 3.69, P = 0.035) but no effect of the KORD or sex or any other interactions between the variables (Ps > 0.35); however, post hoc t-tests show no differences between males and females in each 15 min time bin (Ps > 0.35). **c,** Total distance during the OF test. Three-way RM-ANOVA: main effect of time ($F_{1.7,28.8}$ = 116.6, P < 0.0001) and a sex x KORD interaction ($F_{1,17}$ = 7.06, P = 0.017) but no effect of the KORD or sex or any other interactions between the variables (Ps > 0.05); post hoc t-tests show a significant difference between CON and KORD females only during the first 15 min time bin (t_8 = 3.28, adjusted *P = 0.033; other Ps > 0.05) and no differences between CON and KORD males (all adjusted Ps > 0.55).

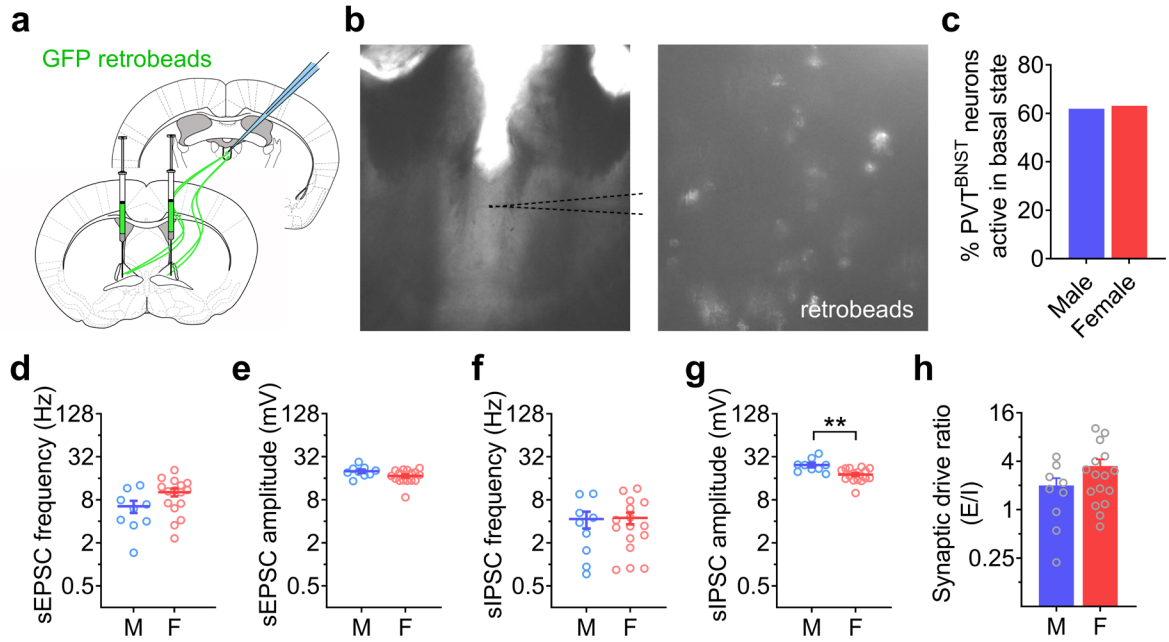

Extended Data Fig. 3: Electrophysiological characterization of PVT^{BNST} neurons. a, Retrograde labeling strategy used to identify and perform electrophysiology recordings in BNST-projecting PVT (PVT^{BNST}) neurons. **b,** Representative image of a coronal PVT brain slice at 4x (left) containing GFP retrobead-positive cell bodies shown magnified at 40x (right) using monochrome camera on the slice electrophysiology rig. **c,** Percentage of PVT^{BNST} neurons sampled that are active in their basal state (n = 8 male mice, 22 cells; n = 6 female mice, 19 cells). **d-h**, Synaptic transmission measures from PVT^{BNST} neurons (n = 4 male mice, 9 cells; n = 5 female mice, 16 cells; unpaired t-tests). **d,** sEPSC frequency (t_{23} = 1.87, P = 0.075). **e,** sEPSC amplitude (t_{23} = 1.86, P = 0.075). **f,** sIPSC frequency (t_{23} = 0.20, P = 0.840). **g,** sIPSC amplitude (t_{23} = 3.45, **P= 0.002). **h,** Synaptic drive ratio (t_{22} = 0.79, P = 0.438 with Welch's correction).

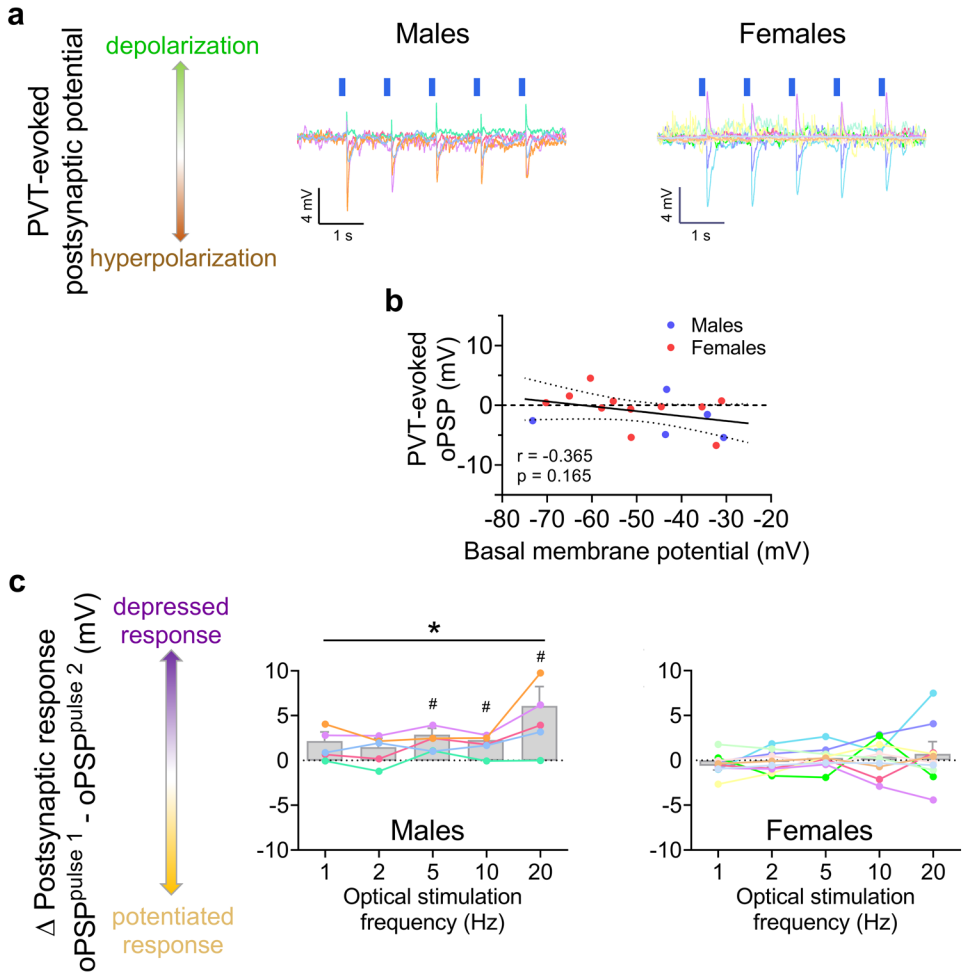

Extended Data Fig. 4: Effect of PVT input stimulation on membrane potential and plasticity in postsynaptic responses in BNST^{CRF} neurons. a, Postsynaptic potentials in BNST^{CRF} neurons elicited by optical stimulation of ChR2 in PVT input terminals (oPSPs), using current-clamp whole-cell recordings following the same viral strategy as shown in **Fig. 3a**. Overlaid traces from all BNST^{CRF} neurons recorded during 1 Hz stimulation with 490 nm LED (indicated by blue lines) demonstrate a range of postsynaptic responses between individual neurons, with upward deflections indicating depolarizations and downward deflections indicating hyperpolarizations. **b,** Scatterplot with linear regression showing that most responses to optically-evoked PVT synaptic input were hyperpolarizations (quantified values for traces depicted in **a**), regardless of basal membrane potential. This results in a lack of correlation between basal membrane potential and PVT-evoked oPSP within individual neurons. Linear regression equation: Y = -0.08152*X - 5.063; Pearson's r = -0.365, P = 0.165. **c,** Differences between the oPSP elicited from the first light pulse and second light pulse across a range of stimulation frequencies within the same BNST^{CRF} neurons, with positive delta values indicating depressed responses and negative delta values indicating potentiated responses (n= 2 male mice, 5 cells; 5 female mice, 11 cells). Bar graphs show that a depression emerges at higher stimulation frequencies in males but not females. Males (middle): one-way RM-ANOVA ($F_{1.4,5.7}$ = 8.26, *P = 0.025), with one-sample t-tests for delta values at each frequency against the null hypothesis delta value of 0 showing a significant depression at 5 Hz (t_4 = 4.07, $^{\#}P$ = 0.015), 10 Hz (t_4 = 3.51, $^{\#}P$ = 0.025), and 20 Hz (t_4 = 2.84, $^{\#}P$ = 0.047), but not 1 Hz or 2 Hz (Ps > 0.05). Females (right): one-way RM-ANOVA ($F_{1.9,7.8}$ = 2.76, *P= 0.125) and one-sample t-tests show no significant effects (all Ps > 0.20). Importantly, current-clamp recordings from inactive or manually hyperpolarized ChR2+ PVT neurons in this preparation confirmed that 1 ms pulses of 490 nM LED reliably elicited time-locked action potentials with 100% fidelity with a stimulation frequency up to 50 Hz, the maximum endogenous burst firing rate observed for this population (data not shown).

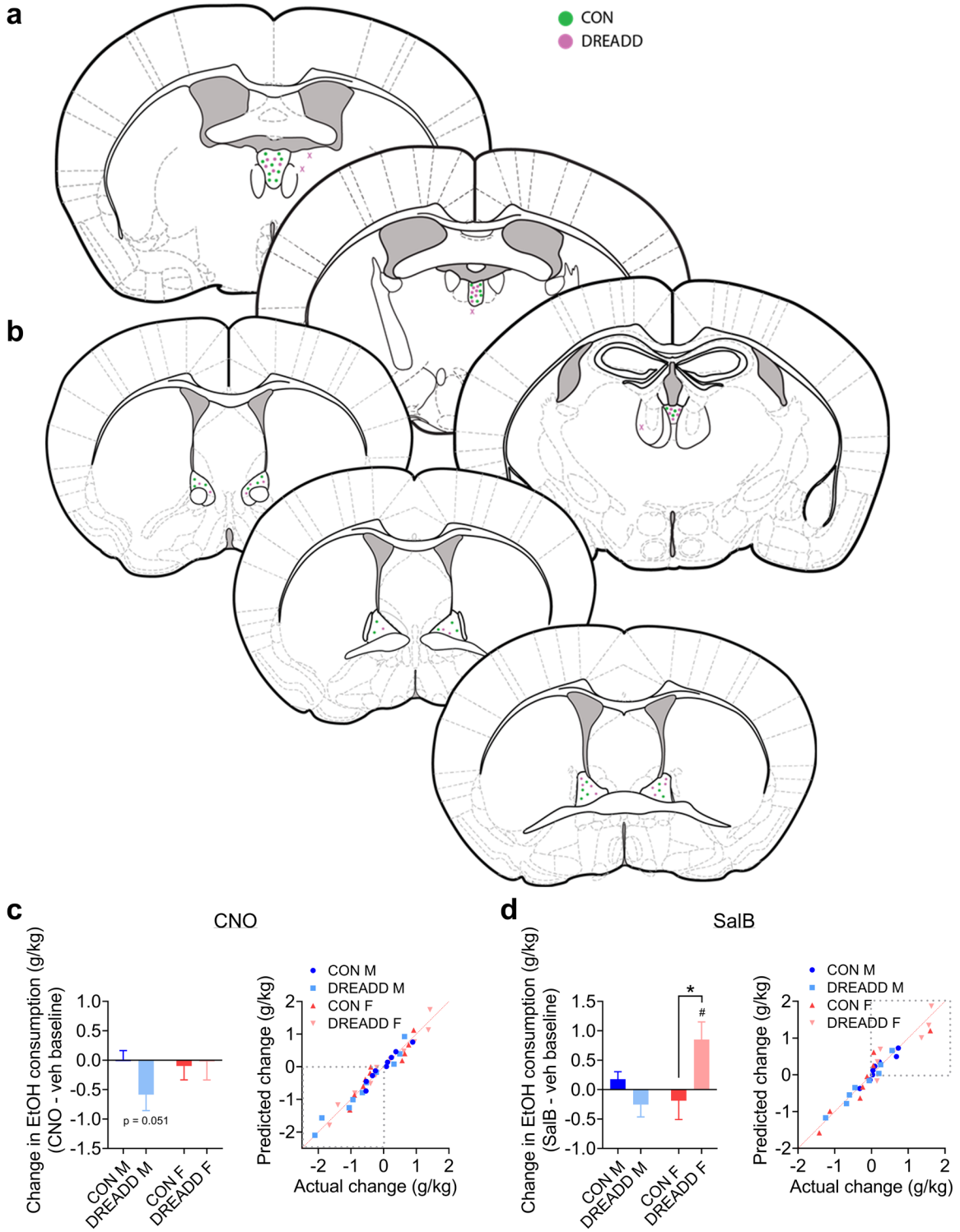

Extended Data Fig. 5: Hit maps for the multiplexed chemogenetic strategy and additional analyses of chemogenetic manipulation effects on binge alcohol drinking (related to Fig. 3g-j), Viral injection placements in PVT (**a**) and BNST (**b**) for **Fig. 3g**, with hits indicated with circles and misses excluded from analysis in X's. **c-d**, Quantification of the difference between Day 4 (following CNO or SalB administration) and vehicle baseline DID alcohol consumption shown in **Fig. 3i and j** to directly compare the change magnitude between CON and DREADD groups as complementary analysis to those shown in **Fig. 3**. **c**, Left: t-tests between CON and DREADD mice within sex comparing the CNO-induced change in drinking show no differences in either sex (*P*s > 0.20). However, one-sample t-tests within each group comparing the change to the null hypothesis delta value of 0 show a trend for a decrease in DREADD males (t_{10} = 2.18, *P* = 0.055) but no change in other groups (*P*s > 0.65), suggesting that activation of the Gq-DREADD in PVT^{BNST} neurons may be sufficient to reduce binge drinking in a subpopulation of DREADD males. Right: QQ plots comparing actual

change to predicted change in alcohol consumption, demonstrating that all groups' data come from the same distribution in raw space. The lower left quadrant is outlined with a dashed line to illustrate that it is represented primarily by DREADD M data. **d**, Left: Supporting the results shown in **Fig. 3j**, one-sample t-tests within each group show that only DREADD females have a significant SalB-induced increase in binge drinking (DREADD F: $t_5 = 2.83$, $^{\#}P = 0.037$; all other Ps > 0.20). In addition, t-tests between CON and DREADD mice within sex comparing the SalB-induced change in drinking show that the change in DREADD F is significantly larger than that in CON F ($t_{26} = 2.85$, adjusted $^{*}P = 0.017$), but this is not the case for males (adjusted $P > 0.20$). Right: QQ plots comparing actual change to predicted change in alcohol consumption, demonstrating that all groups' data come from the same distribution in raw space. The upper right quadrant is outlined with a dashed line to illustrate that it is represented primarily by DREADD F data.

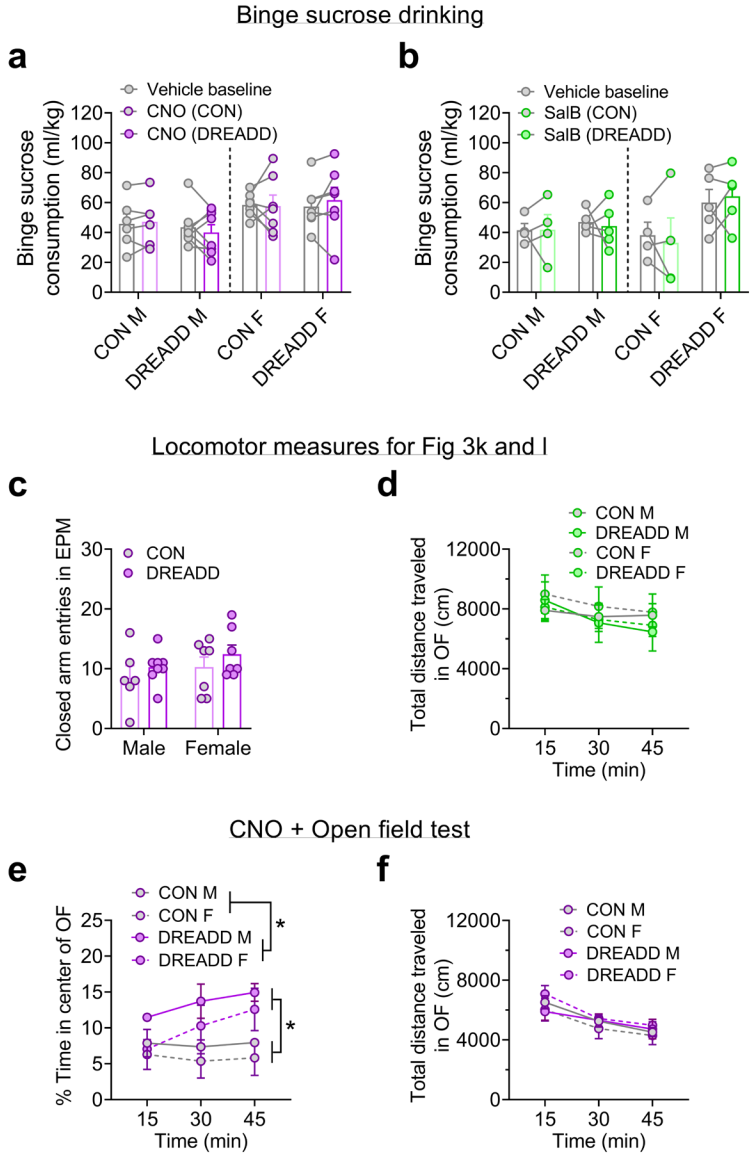

Extended Data Fig. 6: Effects of multiplexed chemogenetic manipulation of the PVT^{BNST} pathway on additional behavioral measures (related to Fig. 3). a-b, Two-hr binge consumption of 1% sucrose in the DID paradigm is unaffected by CNO (5 mg/kg) activation of the Gq-DREADD (**a**) and SalB (17 mg/kg) activation of the Gi-KORD (**b**) in PVT^{BNST} neurons. **a**, Three-way RM-ANOVA examining the effect of CNO on binge sucrose consumption shows a main effect of sex ($F_{1,24}$ = 6.77, P = 0.016) but no other effects or interactions (Ps > 0.30), demonstrating that females consume more sucrose than males but CNO has no impact on consumption. N's = 6 CON M, 8 DREADD M, 7 CON F, 7 DREADD F. **b**, Three-way RM-ANOVA ANOVA examining the effect of SalB on binge sucrose consumption reveals no effects or interactions (Ps > 0.05). **c**, While DREADD mice displayed greater open arm exploration in the EPM than CONs following CNO administration (**Fig. 3k**), the number of closed arm entries did not differ: two-way ANOVA shows no effects of or interaction between sex and DREADD (Ps > 0.20). **d**, Distance traveled on the OF is not affected by SalB administration (related to **Fig. 3l**): three-way RM-ANOVA shows a main effect of time ($F_{1.2,17.4}$ = 16.1, P = 0.0005, not indicated), but no other effects or interactions (Ps > 0.10). N's = 4 CON M, 5 DREADD M, 4 CON F, 5 DREADD F. **e-f**, CNO administration decreases avoidance of the center of the OF in DREADD mice without altering locomotion, confirming the anxiolytic effect in the EPM in **Fig. 3k**. **e**, Three-way RM-ANOVA on the percent time spent in the center of the OF shows main effects of DREADD ($F_{1,7}$ = 8.39, *P = 0.023) and time ($F_{1.9,13.5}$ = 4.18, P = 0.040, not indicated), and a DREADD x time interaction ($F_{2,14}$ = 5.33, *P = 0.019). f, Three-way RM-ANOVA on the distance traveled shows a main effect of time ($F_{1.5,10.3}$ = 56.18, P < 0.0001, not indicated), but no other effects or interactions (Ps > 0.15). N's = 3 CON M, 3 DREADD M, 3 CON F, 2 DREADD F.

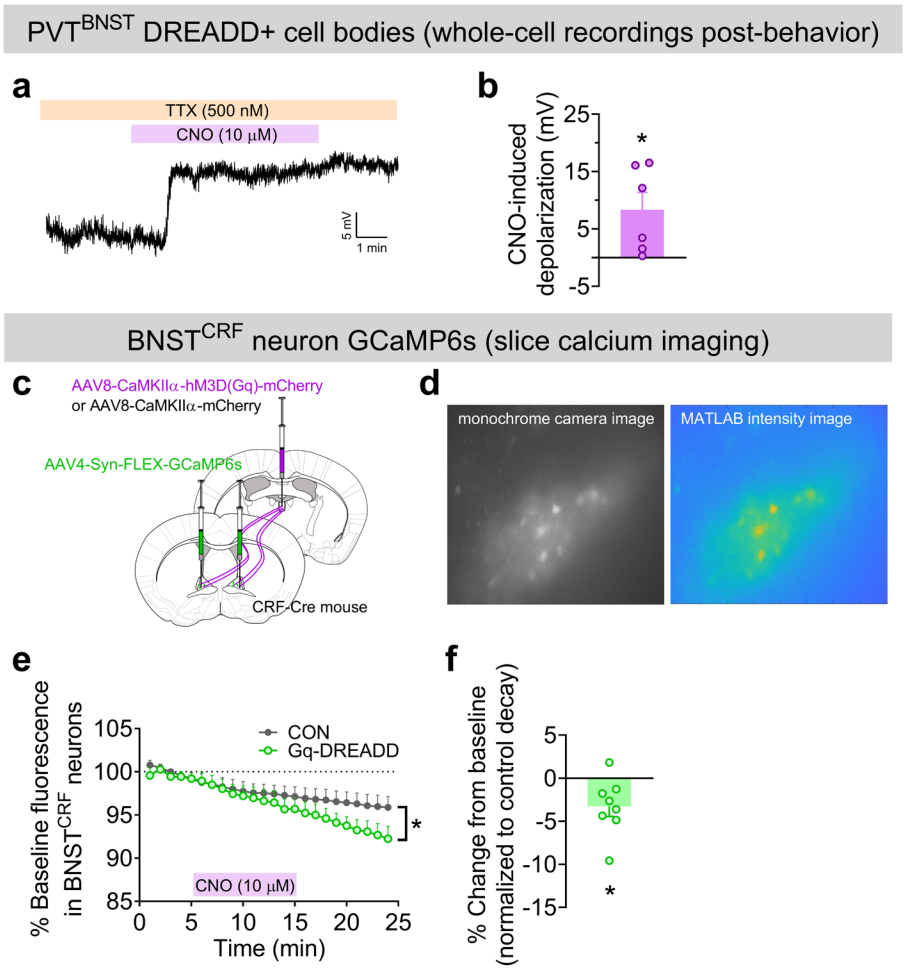

Extended Data Fig. 7: Activation of the Gq-DREADD in PVT^{BNST} neurons depolarizes them and provides a net inhibition of the BNST^{CRF} neuron population in slice preparations. a-b, Following behavioral testing in **Fig. 3 and Extended Data Figs. 5 and 6**, a subset of mice were sacrificed for slice electrophysiology recordings in the PVT. In the presence of TTX to block action potentials, bath application of CNO (10 μM) depolarizes DREADD+ PVT cell bodies, as shown in the trace in **a** and quantified in **b**. One-sample t-test comparing the change in membrane potential to the null hypothesis of 0 mV change: $t_5 = 2.75$, $^*P = 0.040$. **c**, Schematic of the strategy to express the calcium biosensor GCaMP6s specifically in BNST^{CRF} neurons and the excitatory Gq-DREADD (hM3D) or empty control virus in the PVT for *ex vivo* slice calcium imaging experiment in the BNST during bath application of CNO (10 μM) to activate the Gq-DREADD in PVT terminals. **d**, Representative frames from monochrome camera video on the slice rig (left) and intensity heatmap-transformed video in MATLAB (right) of the calcium signal in BNST^{CRF} neurons during slice imaging experiments. **e,** Fluorescence intensity of GCaMP6s+ BNST^{CRF} neurons (normalized to background image intensity), in which data for each minute is normalized to the cell's 5-min baseline. A standard linear decay of the fluorescence signal in BNST^{CRF} neurons is observed when the control virus is in the PVT (CON, gray) and greater decrease in signal when the hM3D virus is in the PVT (Gq-DREADD, green; N's = 1 CON mouse, 6 cells; 2 Gq-DREADD mice, 8 cells). Mixed-effects model: main effect of time ($F_{2.1,24.3} = 18.05$, $P < 0.0001$) and a time x DREADD interaction ($F_{23,271} = 1.66$, $^*P = 0.032$), but no main effect of Gq-DREADD ($P > 0.30$). **f,** Quantified percent change in BNST^{CRF} calcium fluorescence from baseline in mice with the Gq-DREADD in the PVT, normalized to the decay measured in the control virus cells; a one-sample t-test ($t_7 = 2.82$, $^*P = 0.026$) shows a significantly decreased signal compared to decrease in control cells during the last five min of the experiment.

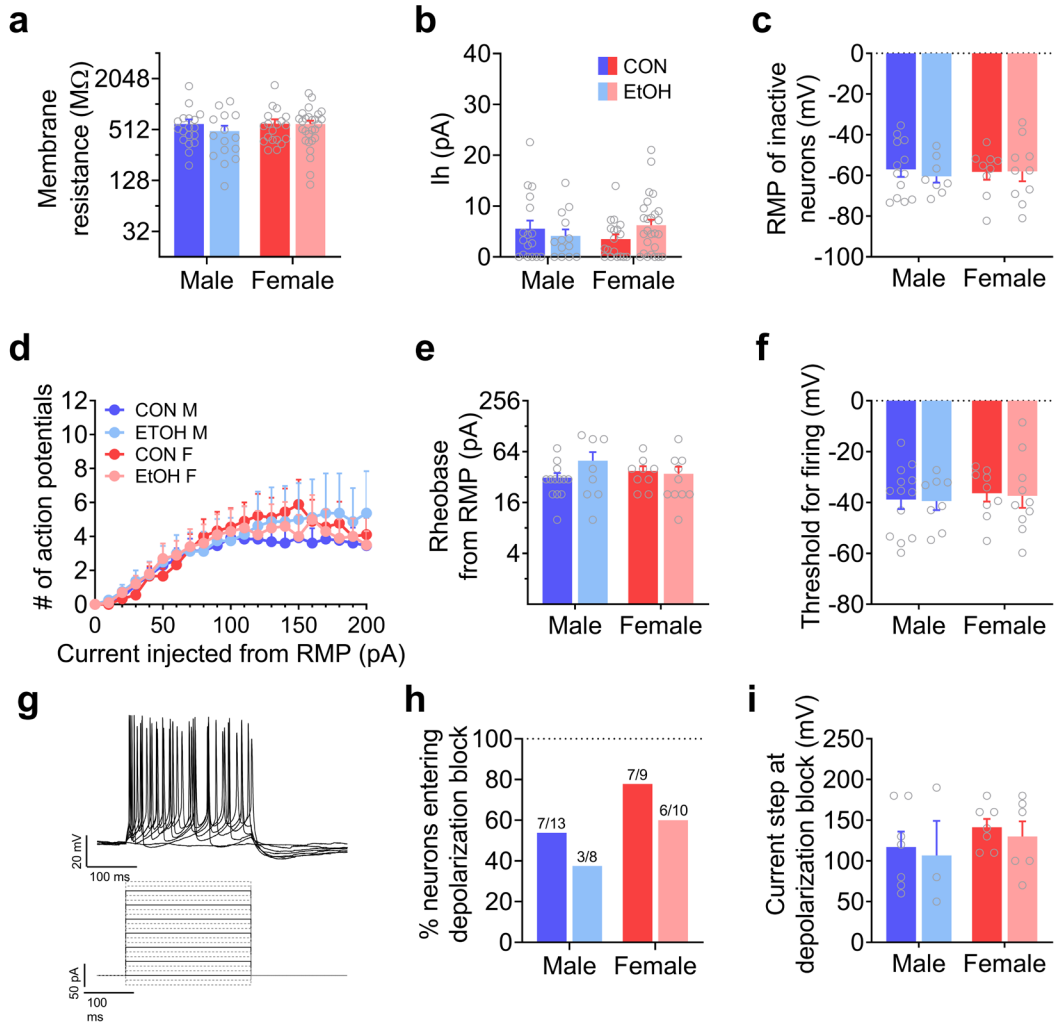

Extended Data Fig. 8: Effects of sex and alcohol on neuronal excitability in BNST^{CRF} neurons at RMP. a, Membrane resistance measured from an I-V plot in voltage clamp configuration with hyperpolarizing steps. Two-way ANOVA: no effects (*P*s > 0.25). **b,** Hyperpolarization-activated depolarizing current (I_h) measured in the I-V plot. Two-way ANOVA: no effects (*P*s > 0.10). **c,** Resting membrane potential (RMP) of neurons that were not displaying a basal state of activity (firing) during gap-free recordings in current-clamp configuration with no current manipulation. Two-way ANOVA: no effects (*P*s > 0.65). **d-h**, Measures from a V-I plot in current clamp configuration in which increasing 10 pA steps of current were injected directly into basally inactive cells from their RMP (cells identified and represented in **c**) to induce firing, from -20 pA to 200 pA across sweeps. **d**, Number of action potentials generated across current steps (top), with representative traces from one cell (middle) corresponding to solid lines in the stimulus waveform protocol depicted (bottom). Three-way ANOVA: main effect of current step ($F_{2, 71.3} = 25.57$, $P < 0.0001$) but no other effects or interactions (*P*s > 0.60). **e,** Rheobase (minimum amount of current required to elicit an action potential). Two-way ANOVA: no effects (*P*s > 0.20). **f**, Voltage threshold for firing. Two-way ANOVA: no effects (*P*s > 0.55). **g**, Representative trace (above) and stimulus protocol (below) for a V-I plot conducted in BNST^{CRF} neurons at RMP. **h-i**, Proportion of neurons that enter depolarization block within the I-V plot (**h**) and the step at which this occurs (**i**; two-way ANOVA: no effects (*P*s > 0.25)). The same lack of effects was observed when a ramp current injection protocol was employed (data not shown). N's = 9 CON M mice, 18 cells; 6 EtOH M mice, 15 cells; 9 CON F mice, 20 cells; 11 EtOH F mice, 27 cells. Tonically active cells were excluded from analysis for measures in **c-i**.

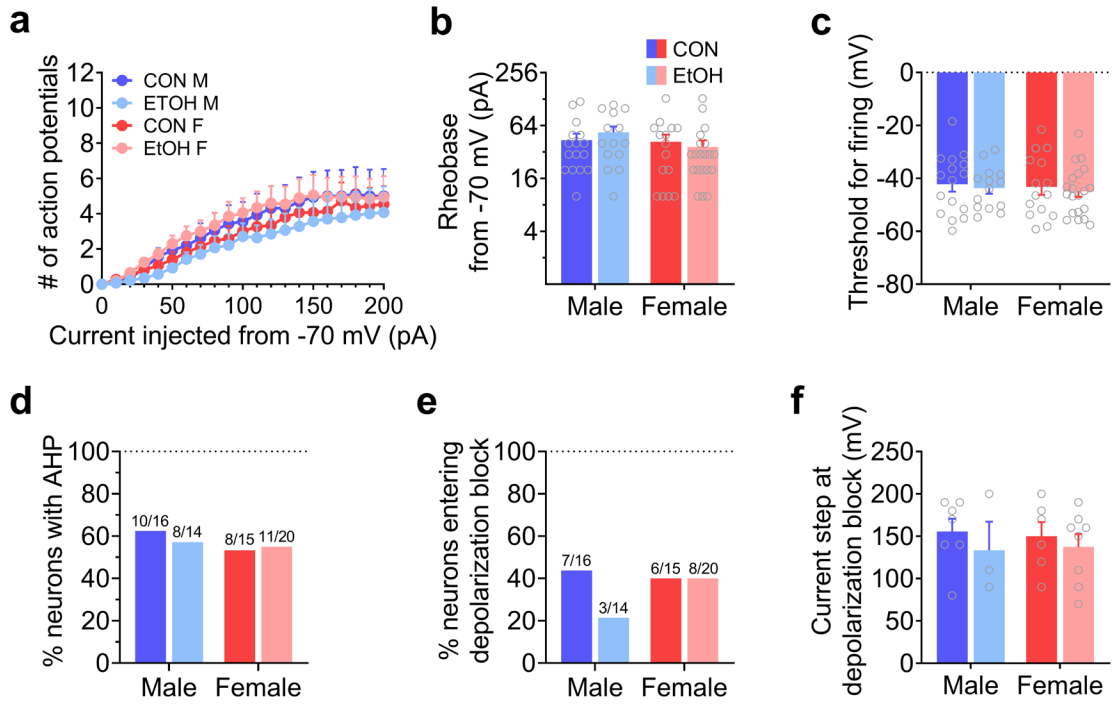

Extended Data Fig. 9: Effects of sex and alcohol on neuronal excitability in BNST^{CRF} neurons when held at a common hyperpolarized membrane potential of -70 mV. a, Number of action potentials generated across current steps during a V-I plot starting at a holding potential of -70 mV in all neurons except those displaying firing at this potential (same as **Extended Data Fig. 8 d-i** but starting from -70 mV holding potential). Three-way ANOVA: main effect of current step ($F_{1.4,82.8} = 38.32$, $P < 0.0001$) but no other effects or interactions (*P*s > 0.25). **b,** Rheobase. Two-way ANOVA: no effects (*P*s > 0.10). **c,** Voltage threshold for firing. Two-way ANOVA: no effects (*P*s > 0.50). **d,** Percentage of neurons displaying an after-hyperpolarization potential (AHP) following action potentials elicited by current injection during the V-I plot. **e-f**, Proportion of neurons that enter depolarization block within the I-V plot (**e**) and the step at which this occurs (**f**; two-way ANOVA: no effects (*P*s > 0.35)). The same lack of effects was observed when a ramp current injection protocol was employed (data not shown). Total starting N's are the same as **Extended Data Fig. 8** prior to exclusion based on firing activity at -70 mV.

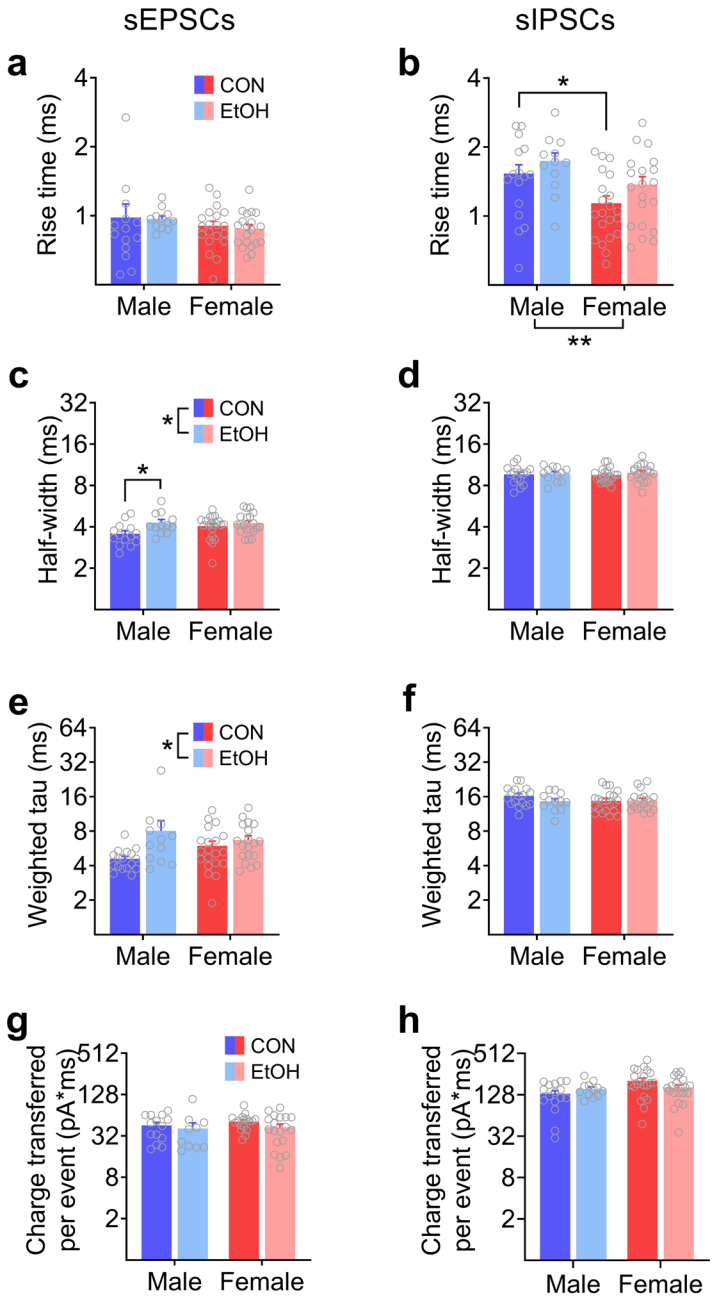

Extended Data Fig. 10: Sex differences and alcohol-induced plasticity in sPSC kinetics in BNST^{CRF} neurons (related to Fig. 4). a, sEPSC rise time. Two-way ANOVA: no effects or interactions (*P*s > 0.30). **b,** sIPSC rise time. Two-way ANOVA: main effect of sex ($F_{1,65}$ = 9.59, ***P* = 0.003) but no other effects (*P*s > 0.05), with a post hoc t-test confirming a sex difference between controls (t_{65} = 2.37, **P* = 0.021). **c,** sEPSC half-width. Two-way ANOVA: main effect of alcohol ($F_{1,62}$ = 6.48, **P* = 0.013) but no other effects (*P*s > 0.15); post hoc t-tests with H-S correction show an effect of alcohol in males (t_{62} = 2.52, adjusted **P* = 0.028) but not females (*P* > 0.35). **d,** sIPSC half-width. Two-way ANOVA: no effects (*P*s > 0.40). **e,** sEPSC weighted tau. Two-way ANOVA: main effect of EtOH ($F_{1,63}$ = 6.13, **P* = 0.016) but no other effects (*P*s > 0.15); post hoc t-tests show that the effect of EtOH was not significant in either sex (*P*s > 0.05). **f,** sIPSC weighted tau. Two-way ANOVA: no effects (*P*s > 0.20). **g,** sEPSC charge transferred per event, calculated as average area per sEPSC. Two-way ANOVA: no effects (*P*s > 0.05). **h,** sIPSC charge transferred per event. Two-way ANOVA: no effects (*P*s > 0.05). For all analyses, cells with an average amplitude of 5 pA or lower after filtering were excluded from analysis—for sEPSCs: 3 CON M, 1 EtOH M, 1 EtOH F; for sIPSCs: 1 CON M, 1 EtOH F. In addition, 0-1 cells were excluded because they were outliers. Effects for rise time and half-width in **a-d** were maintained when normalized to the PSC amplitude (data not shown).

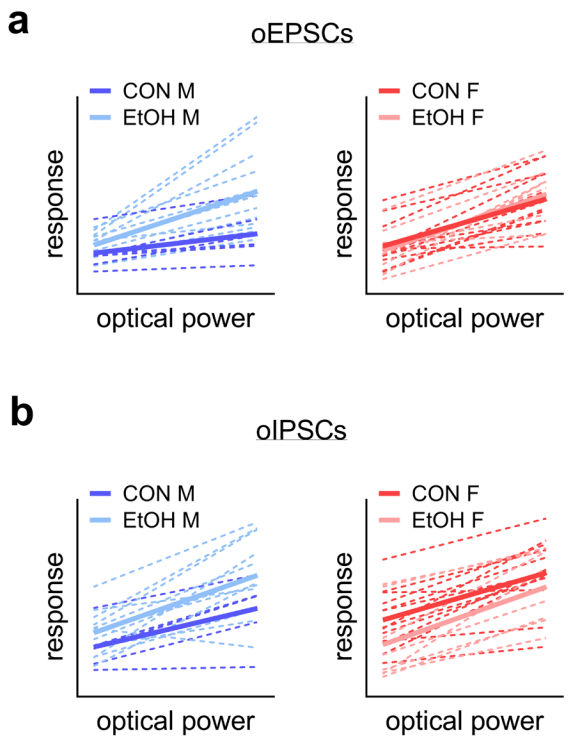

Extended Data Fig. 11: Linear regressions for oPSC initial slope (related to Fig. 4j,l). a, Linear regression for PVT-evoked oEPSCs across 5, 10, and 25% LED power in BNST^{CRF} neurons of males (left) and females (right), with dashed lines showing fits for individual cells and solid lines showing the group average. Regression equations were: Con M (Y = 0.03946*X + 1.462), EtOH M (Y = 0.1095*X + 1.438), CON F (Y = 0.09632*X + 1.461), EtOH F (Y = 0.1137*X + 1.209), illustrating that the low initial slope in CON M (quantified in **Fig. 4j**).**b,** Linear regression for PVT-evoked oIPSCs across 5, 10, and 25% LED power in BNST^{CRF} neurons of males (left) and females (right), with dashed lines showing fits for individual cells and solid lines showing the group average. Regression equations were: Con M (Y = 0.07869*X + 1.624), EtOH M (Y = 0.1170*X + 2.013), CON F (Y = 0.09628*X + 2.634), EtOH F (Y = 0.1178*X + 1.523).

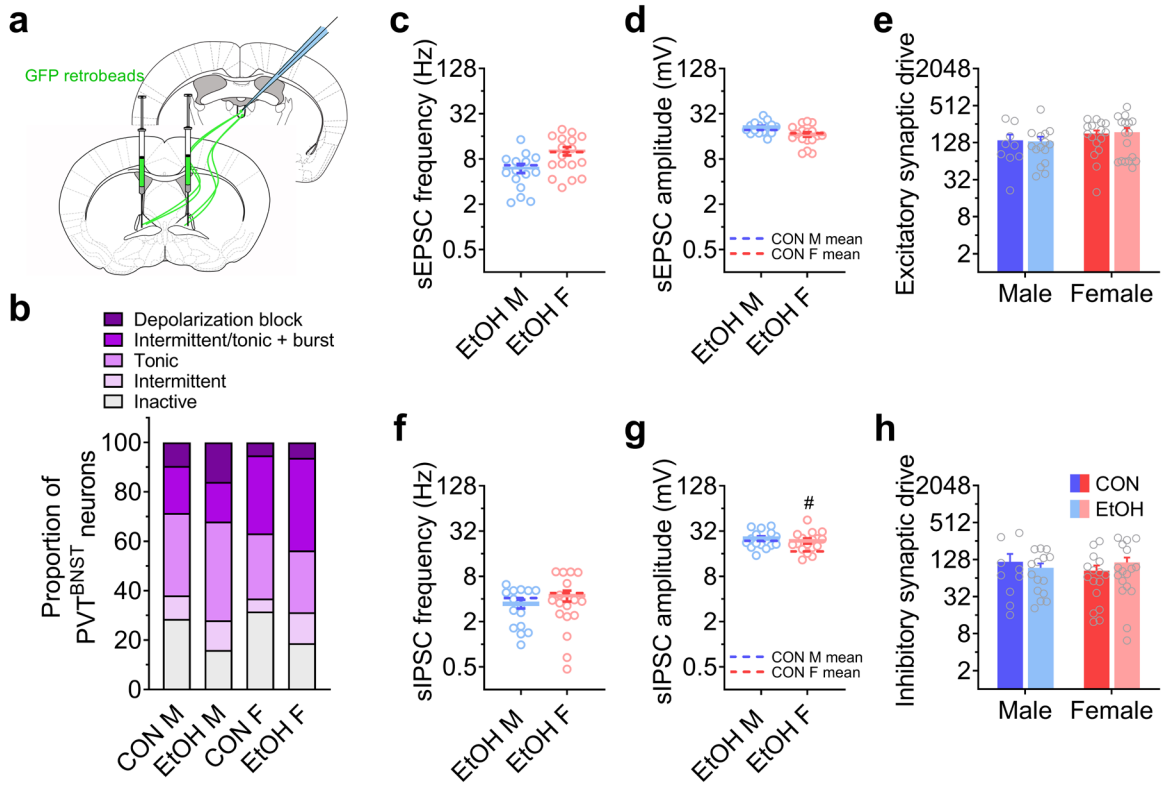

Extended Data Fig. 12: Effects of sex and alcohol on synaptic transmission in PVT^{BNST} neurons. a, Schematic showing strategy to label PVT^{BNST} neurons for electrophysiology recordings following 3-cycle DID. **b,** Characterization of the types of neuronal activity in PVT^{BNST} neurons, presented as % sampled population, showing that the population is extremely excitable in all groups. N's = 8 CON M mice, 22 cells; 8 EtOH M mice, 25 cells; 6 CON F mice, 19 cells; 6 EtOH F mice, 16 cells. **c-d**, sEPSC frequency (**c**) and amplitude (**d**) in PVT^{BNST} neurons in EtOH M and EtOH F mice, with dashed lines indicating the means in water CON M and F from **Extended Data Fig. 3**. Unpaired t-tests evaluating the effect of EtOH within sex show no effects in either sex for sEPSC frequency (CON M vs. EtOH M: $t_{22} = 0.14$, $P = 0.887$; CON F vs. EtOH F: $t_{31} = 0.13$, $P = 0.990$) or amplitude (CON M vs. EtOH M: $t_{22} = 0.58$, $P = 0.565$; CON F vs. EtOH F: $t_{31} = 0.32$, $P = 0.753$). **e,** Excitatory synaptic drive, calculated as sEPSC frequency x sEPSC amplitude, within individual neurons. Two-way ANOVA: no effects (Ps > 0.55). **f-g**, sIPSC frequency (**f**) and amplitude (**g**) in the same PVT^{BNST} neurons in **c** and **d**. Unpaired t-tests evaluating the effect of EtOH within sex show no effects on sIPSC frequency (CON M vs. EtOH M: $t_{22} = 0.111$, $P = 0.912$; CON F vs. EtOH F: $t_{31} = 0.011$, $P = 0.991$), but an effect on sIPSC amplitude in females but not males (CON M vs. EtOH M: $t_{22} = 0.175$, $P = 0.863$; CON F vs. EtOH F: $t_{31} = 2.69$, $^{\#}P = 0.011$). **h**, Inhibitory synaptic drive, calculated as sIPSC frequency x sIPSC amplitude, within individual neurons. Two-way ANOVA: no effects (Ps > 0.70). For **c-h**, N's = 4 CON M mice, 9 cells; 5 EtOH M mice, 15 cells; 5 CON F mice, 16 cells; 6 EtOH F mice, 17 cells.

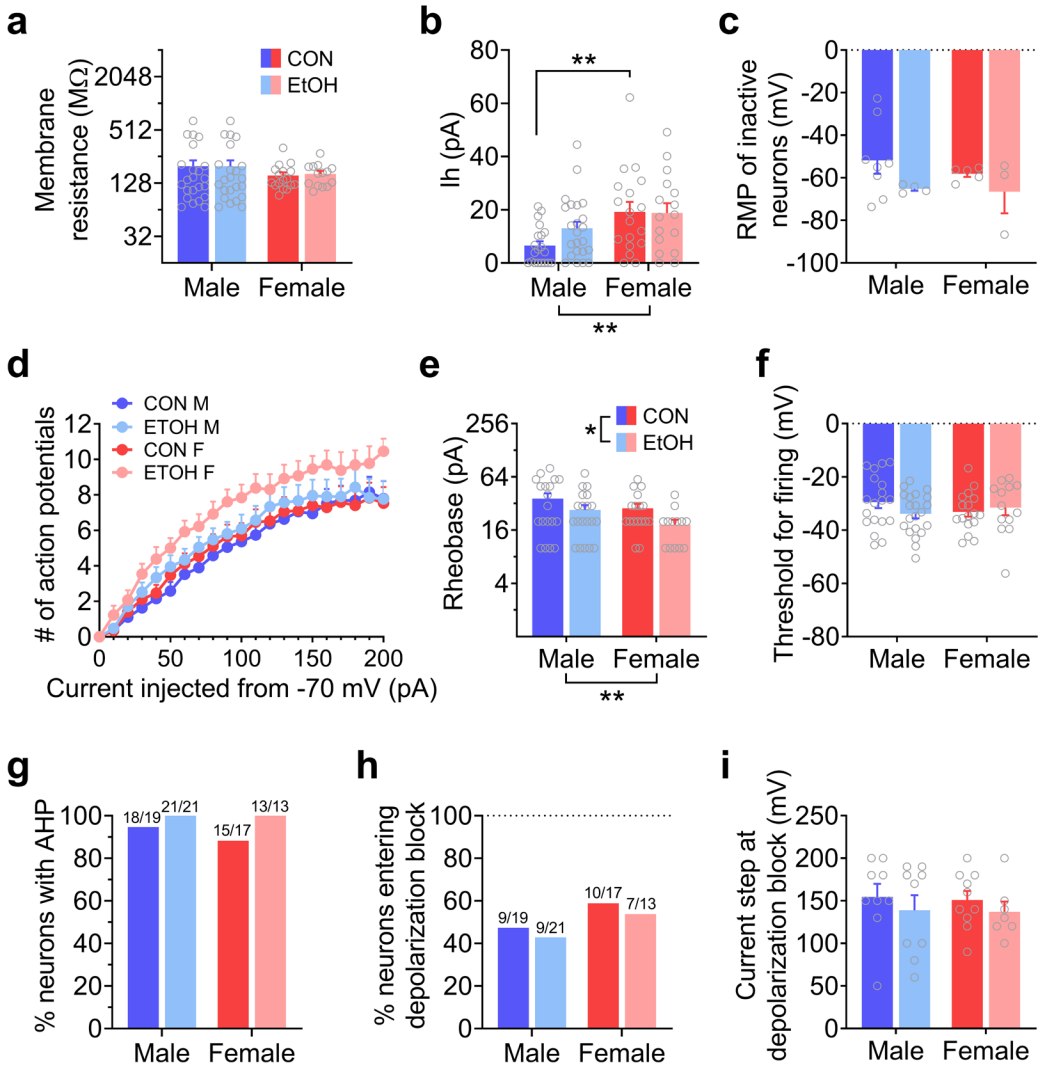

Extended Data Fig. 13: Effects of sex and alcohol on neuronal excitability in PVT^{BNST} neurons. a, Membrane resistance measured from an I-V plot in voltage clamp configuration with hyperpolarizing steps. Two-way ANOVA: no effects (*P*s > 0.80). **b,** Hyperpolarization-activated depolarizing current (Ih) measured in the I-V plot. Two-way ANOVA: main effect of sex ($F_{1,73}$ = 10.19, ***P* = 0.002); a post hoc t-test confirms a sex difference between CON M and F (t_{73} = 3.11, ***P* = 0.003). **c,** Resting membrane potential (RMP) of neurons that were not displaying a basal state of activity (firing) during gap-free recordings in current-clamp configuration with no current manipulation. Two-way ANOVA: no effects (*P*s > 0.10). **d-i**, Measures from a V-I plot in current clamp configuration in which increasing 10 pA steps of current were injected, starting at a holding potential of -70 mV, in all neurons except those displaying firing at this potential (as in **Extended Data Fig. 9**). **d**, Number of action potentials generated across current steps. Three-way ANOVA: main effect of current step ($F_{2.5, 164}$ = 158.8, *P* < 0.0001) and trend of alcohol ($F_{1,66}$= 3.87, *P* = 0.054) but no other effects (*P*s > 0.15). **e,** Rheobase. Two-way ANOVA: main effect of alcohol ($F_{1,65}$ = 5.32, **P* = 0.024) and main effect of sex ($F_{1,65}$ = 4.03, **P* = 0.049) but no interaction (*P* > 0.95), with post hoc t-tests showing the effect of alcohol was not driven by one sex (adjusted *P*s > 0.15). **f**, Voltage threshold for firing. Two-way ANOVA: no effects (*P*s > 0.10). **g,** Proportion of neurons displaying an after-hyperpolarization potential (AHP) following action potentials elicited by current injection during the V-I plot. **h-i**, Proportion of neurons that enter depolarization block within the V-I plot (**h**) and the step at which this occurs (**i**; two-way ANOVA: no effects (*P*s > 0.30)). N's = 8 CON M mice, 22 cells; 8 EtOH M mice, 25 cells; 6 CON F mice, 19 cells; 6 EtOH F mice, 16 cells. Tonically active cells were excluded from analysis for measures in **c-i**.